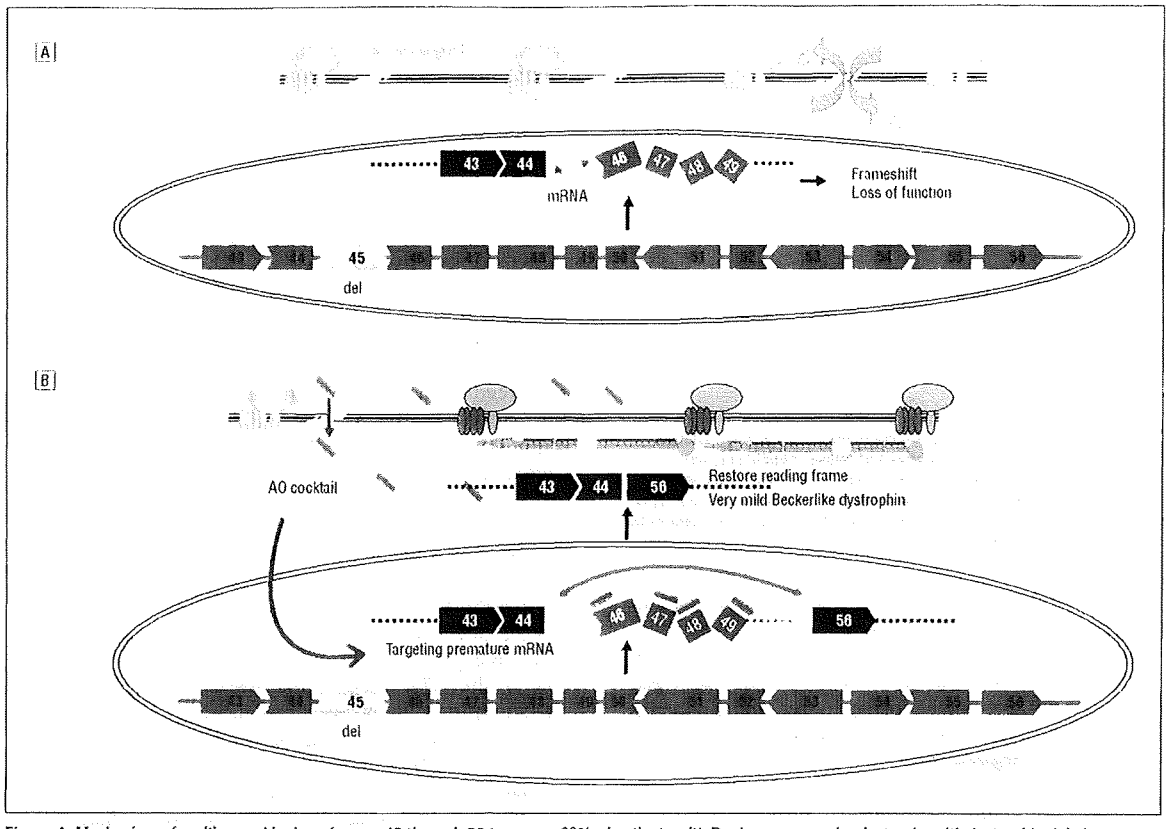

Figure 4. Mechanism of multiexon skipping of exons 45 through 55 to rescue 60% of patients with Duchenne muscular dystrophy with dystrophin deletions. A, More than 60% of deletion mutations of the dystrophin gene occur within the hot-spot range of exons 45 through 55 (exon 45 is deleted in this schematic [del]) in Duchenne muscular dystrophy muscles. The messenger RNA (mRNA) of remaining exons is spliced together but the reading frame is disrupted, resulting in failure of the production of functional dystrophin protein. CK indicates creatine kinase; Ca^{2+}, calcium ions. B, An antisense oligonucleotide (AO) cocktail targeting exons 45 through 55 likely enters the Duchenne muscular dystrophy muscle through its leaky membranes, then binds to the dystrophin mRNA in a sequence-specific manner. The AOs block the splicing machinery and prevent inclusion of all exons between exons 45 and 55. Skipping these exons restores the reading frame of mRNA, allowing production of quasi-dystrophin containing exons 1 through 44 and exons 56 through 79, which is not normal but likely retains considerable function as evidenced by patients with clinically milder Becker muscular dystrophy with identical partial dystrophin.

may not accurately assess off-target toxic effects of AOs for human use.

Perhaps the largest challenge facing implementation of exon-skipping therapy for DMD is in developing new approaches to toxicity testing and clinical trial regulatory procedures that are relevant and appropriate for sequence-specific drugs. The pharmaceutical industry often quotes a price tag of $500 million to bring any new drug to the market. Given the discussion earlier, implementation of AO drugs in DMD will require many exon-specific drugs. If the $500 million is assessed for each individual AO sequence, then both time and money become insuperable barriers to helping the existing generation of boys with DMD. The silver lining in this cloud is the lack of any detectable toxic effects with PMO AO drugs to date. If multiple AOs all show a lack of long-term toxic effects, then there is hope that specific AO drugs could be approved with more limited toxicological and phase 1 testing.

A practical resolution of this problem is to consider each component of the potential toxic effects of these highly targeted drugs individually. Tests of the generic toxic effects of morpholinos at the doses at which they are likely to be functionally effective could be conducted quite straightforwardly with either a scrambled or arbitrary sequence of a particular molecular weight. It is the notion of individual sequence-specific toxic effects that raises problems. The argument that any specific sequence may have off-target effects (eg, binding to utrophin transcripts) cannot be properly tested in other species because they may have different potential off-target sequences as compared with those in humans. This carries the dire implication that a lack of sequence-specific toxic effects in a test species can provide no assurance, indeed no information at all, as to the sequence's safety in humans. Tests in healthy human volunteers are also problematic. Ethical issues arise from the possible generation of a pathogenic frameshift in healthy muscle by successful suppression of the targeted exon. Moreover, the lack of innate pathological abnormalities in healthy human muscle would stifle access of the AO to its intended intramuscular target while at the same time providing a different spectrum of potential off-target molecules (eg, utrophin transcripts). A further complication arises from the individualistic nature of the entire rationale, for it precludes the possibil-

ity of learning from experience; the probability that any given sequence may be toxic is independent of the number of safe experiences with other sequences. In effect, for safety, we can test for sequence-specific toxic effects only in human volunteers with DMD by progressive dose escalation. Only in this way would the reagents have access to their intended targets as well as any unintended targets in a physiological context that is inappropriately modeled both in other species and in healthy human volunteers.

Accepted for Publication: April 15, 2008.
Correspondence: Eric P. Hoffman, PhD, Research Center for Genetic Medicine, Children's National Medical Center, 111 Michigan Ave NW, Washington, DC 20010 (ehoffman@cnmcresearch.org).
Author Contributions: *Study concept and design:* Yokota, Takeda, Partridge, and Hoffman. *Acquisition of data:* Yokota and Lu. *Analysis and interpretation of data:* Yokota, Nakamura, and Hoffman. *Drafting of the manuscript:* Yokota, Partridge, Nakamura, and Hoffman. *Critical revision of the manuscript for important intellectual content:* Takeda, Lu, and Partridge. *Obtained funding:* Hoffman. *Administrative, technical, and material support:* Lu. *Study supervision:* Yokota, Takeda, Partridge, Nakamura, and Hoffman.
Financial Disclosure: None reported.
Funding/Support: This work was supported by the Foundation to Eradicate Duchenne, Jane Foundation, the Muscular Dystrophy Association, and a collaborative grant from the National Institutes of Health Wellstone Muscular Dystrophy Research Centers (http://www.wellstone-dc.org).

REFERENCES

1. Spiegelman WG, Reichardt LF, Yaniv M, Heinemann SF, Kaiser AD, Eisen H. Bidirectional transcription and the regulation of phage lambda repressor synthesis. *Proc Natl Acad Sci U S A.* 1972;69(11):3156-3160.
2. Kumar M, Carmichael GG. Antisense RNA: function and fate of duplex RNA in cells of higher eukaryotes. *Microbiol Mol Biol Rev.* 1998;62(4):1415-1434.
3. Gitlin L, Karelsky S, Andino R. Short interfering RNA confers intracellular antiviral immunity in human cells. *Nature.* 2002;418(6896):430-434.
4. Kim SK, Wold BJ. Stable reduction of thymidine kinase activity in cells expressing high levels of anti-sense RNA. *Cell.* 1985;42(1):129-138.
5. Warfield KL, Swenson DL, Olinger GG, et al. Gene-specific countermeasures against Ebola virus based on antisense phosphorodiamidate morpholino oligomers. *PLoS Pathog.* 2006;2(1):e1. doi:10.1371/journal.ppat.0020001.
6. Hoffman EP, Brown RH Jr, Kunkel LM. Dystrophin: the protein product of the Duchenne muscular dystrophy locus. *Cell.* 1987;51(6):919-928.
7. Hoffman EP. Skipping toward personalized molecular medicine. *N Engl J Med.* 2007;357(26):2719-2722.
8. Dunckley MG, Villiet P, Eperon IC, Dickson G. Modification of splicing in the dystrophin gene in cultured *Mdx* muscle cells by antisense oligoribonucleotides. *Hum Mol Genet.* 1998;7(7):1083-1090.
9. van Deutekom JC, Janson AA, Ginjaar IB, et al. Local dystrophin restoration with antisense oligonucleotide PRO051. *N Engl J Med.* 2007;357(26):2677-2686.
10. Wheeler TM, Lueck JD, Swanson MS, Dirksen RT, Thornton CA. Correction of ClC-1 splicing eliminates chloride channelopathy and myotonia in mouse models of myotonic dystrophy. *J Clin Invest.* 2007;117(12):3952-3957.
11. Hua Y, Vickers TA, Baker BF, Bennett CF, Krainer AR. Enhancement of *SMN2* exon 7 inclusion by antisense oligonucleotides targeting the exon. *PLoS Biol.* 2007;5(4):e73. doi:10.1371/journal.pbio.0050073.
12. Asparuhova MB, Marti G, Liu S, Serhan F, Trono D, Schumperli D. Inhibition of HIV-1 multiplication by a modified U7 snRNA inducing Tat and Rev exon skipping. *J Gene Med.* 2007;9(5):323-334.
13. Kesari A, Pirra LN, Bremadesam L, et al. Integrated DNA, cDNA, and protein studies in Becker muscular dystrophy show high exception to the reading frame rule. *Hum Mutat.* 2008;29(5):728-737.
14. Yokota T, Duddy W, Partridge T. Optimizing exon skipping therapies for DMD. *Acta Myol.* 2007;26(3):179-184.
15. Covone AE, Lerone M, Romeo G. Genotype-phenotype correlation and germline mosaicism in DMD/BMD patients with deletions of the dystrophin gene. *Hum Genet.* 1991;87(3):353-360.
16. Talkop UA, Klaassen T, Piirsoo A, et al. Duchenne and Becker muscular dystrophies: an Estonian experience. *Brain Dev.* 1999;21(4):244-247.
17. Menhart N. Hybrid spectrin type repeats produced by exon-skipping in dystrophin. *Biochim Biophys Acta.* 2006;1764(6):993-999.
18. Béroud C, Tuffery-Giraud S, Matsuo M, et al. Multiexon skipping leading to an artificial DMD protein lacking amino acids from exons 45 through 55 could rescue up to 63% of patients with Duchenne muscular dystrophy. *Hum Mutat.* 2007;28(2):196-202.
19. Nakamura A, Yoshida K, Fukushima K, et al. Follow-up of three patients with a large in-frame deletion of exons 45-55 in the Duchenne muscular dystrophy (*DMD*) gene. *J Clin Neurosci.* 2008;15(7):757-763.

Transduction Efficiency and Immune Response Associated With the Administration of AAV8 Vector Into Dog Skeletal Muscle

Sachiko Ohshima[1,2], Jin-Hong Shin[1,3], Katsutoshi Yuasa[1,4], Akiyo Nishiyama[1], Junichi Kira[2], Takashi Okada[1] and Shin'ichi Takeda[1]

[1]*Department of Molecular Therapy, National Institute of Neuroscience, National Center of Neurology and Psychiatry, Tokyo, Japan;* [2]*Department of Neurology, Neurological Institute, Graduate School of Medical Sciences, Kyushu University, Fukuoka, Japan;* [3]*Department of Neurology, Graduate School of Medicine, Pusan National University, Busan, Republic of Korea;* [4]*Research Institute of Pharmaceutical Sciences, Faculty of Pharmacy, Musashino University, Tokyo, Japan*

Recombinant adeno-associated virus (rAAV)-mediated gene transfer is an attractive approach to the treatment of Duchenne muscular dystrophy (DMD). We investigated the muscle transduction profiles and immune responses associated with the administration of rAAV2 and rAAV8 in normal and canine X-linked muscular dystrophy in Japan ($CXMD_J$) dogs. rAAV2 or rAAV8 encoding the *lacZ* gene was injected into the skeletal muscles of normal dogs. Two weeks after the injection, we detected a larger number of β-galactosidase-positive fibers in rAAV8-transduced canine skeletal muscle than in rAAV2-transduced muscle. Although immunohistochemical analysis using anti-CD4 and anti-CD8 antibodies revealed less T-cell response to rAAV8 than to rAAV2, β-galactosidase expression in rAAV8-injected muscle lasted for <4 weeks with intramuscular transduction. Canine bone marrow-derived dendritic cells (DCs) were activated by both rAAV2 and rAAV8, implying that innate immunity might be involved in both cases. Intravenous administration of rAAV8-*lacZ* into the hind limb in normal dogs and rAAV8-*microdystrophin* into the hind limb in $CXMD_J$ dogs resulted in improved transgene expression in the skeletal muscles lasting over a period of 8 weeks, but with a declining trend. The limb perfusion transduction protocol with adequate immune modulation would further enhance the rAAV8-mediated transduction strategy and lead to therapeutic benefits in DMD gene therapy.

Received 16 March 2008; accepted 17 September 2008; published online 21 October 2008. doi:10.1038/mt.2008.225

INTRODUCTION

Duchenne muscular dystrophy (DMD) is an inherited disorder causing progressive deterioration of skeletal and cardiac muscles because of mutations in the dystrophin gene. No effective treatment has been established despite the development of various novel therapeutic strategies including pharmacologic and gene therapies. Dystrophin-deficient *mdx* mice and dystrophin-utrophin double-knockout mice are the animal models most widely used to evaluate therapeutic efficacy, although the symptoms of *mdx* mice are not comparable to those of human DMD patients. Dystrophin-deficient canine X-linked muscular dystrophy was found in a golden retriever,[1,2] and we have established a Beagle-based model of canine X-linked muscular dystrophy in Japan ($CXMD_J$) dogs.[3] The clinical and pathological characteristics of the dystrophic dogs are more similar to those of DMD patients than murine models.[3]

The recombinant adeno-associated virus (rAAV) can be used for delivering genes to muscle fibers. Several serotypes of rAAV exhibit a tropism for striated muscles.[4,5] Intramuscular or intravenous administration of rAAV carrying the microdystrophin gene was reported to restore specific muscle force and extend the lifespan in dystrophic mice.[6,7] In contrast to the success of transgene delivery in mice, rAAV2 or rAAV6 delivery to canine striated muscles without immunosuppression resulted in insufficient transgene expression, and rAAV evoked strong immune responses.[8,9] An assay of interferon-γ released from murine and canine splenocytes suggested that the immune responses against rAAV and transgene products in mice and in dogs are dissimilar.[8] Uptake of rAAV2 by human dendritic cells (DCs) and T-cell activation in response to the AAV2 capsid have been reported,[10] indicating that DCs play key roles in the immune response against rAAV-mediated transduction. On the other hand, other serotypes, including rAAV8, that are capable of whole-body skeletal muscle expression after intravenous administration,[4,5] induce less T-cell activation.[11] We hypothesized that the level of activation of canine DCs by rAAV8 might be lower than that achieved by rAAV2. However, the transduction profile and immune response in the rAAV8-injected dog skeletal muscle have not been elucidated.

In this study, we chose to use intramuscular injections under ultrasonographic guidance so as to minimize the inflammatory reaction caused by incisional intramuscular injection.[8] In

Correspondence: *Shin'ichi Takeda or Takashi Okada, Department of Molecular Therapy, National Institute of Neuroscience, National Center of Neurology and Psychiatry, 4-1-1 Ogawa-higashi, Kodaira, Tokyo 187-8502, Japan. E-mail: takeda@ncnp.go.jp or t-okada@ncnp.go.jp*

addition, intravascular delivery was performed as a form of limb perfusion, in an attempt to bypass the immune activation of DCs in the injected muscle.[12] We investigated the transgene expression and host immune response to two distinct serotypes of rAAV in normal and dystrophic dogs after direct intramuscular injection and after limb perfusion.

RESULTS

Extensive expression of β-galactosidase in rAAV8-transduced muscles in wild-type dogs

We administered nonincisional intramuscular injections under ultrasonographic guidance so as to minimize injury. With incisional injection, the ordinary method of intramuscular viral administration in dogs,[8] the skin is opened to identify the individual muscles. This may enhance the immune reaction by recruiting inflammatory cells for wound healing. After nonincisional injection of rAAV2-*lacZ*, faint β-galactosidase (β-gal) expression was detected, whereas lymphocyte infiltration still occurred (**Supplementary Figure S1**). To investigate the transduction efficiency of rAAV8 in canine skeletal muscle, normal dogs were transduced with rAAV-*lacZ* serotypes 2 and 8 (**Table 1**). Prominent expression of β-gal was observed in the rAAV8-*lacZ*-injected muscles, whereas the rAAV2-*lacZ*-injected muscles showed minimal transgene expression (**Figure 1**). While β-gal expression in the rAAV8-injected muscle was correlated with the viral dose, β-gal expression in the rAAV2-injected muscle was not augmented with viral dose escalation. However, rAAV8-*lacZ*-injected muscles, which showed extensive β-gal expression at 2 weeks, also exhibited reduced expression at 4 weeks after the injection, thereby suggesting that the transgene product had immunogenicity (**Supplementary Figure S2**).

To evaluate the difference in transduction efficiency between rAAV2 and rAAV8 at 2 weeks after the injection, relative quantifications of the vector genome and mRNA were performed. The result demonstrated higher transduction rates in the rAAV8-injected muscles as increasing amounts of the vector were administered (**Figure 2a,b**). The amount of protein expression was also well correlated with that of transgenic DNA (**Figure 2c**, **Supplementary Table S1**). Immunohistochemical analysis revealed that the rAAV2-injected muscles showed much more infiltration of $CD4^+$ and $CD8^+$ T lymphocytes in the endomysial space than the rAAV8-injected muscles did (**Figure 3a**). mRNA levels of TGF-β1 and IL-6 (representative markers of inflammation) in the rAAV-injected muscles were standardized with the β-gal expression. rAAV2-injected muscles had higher TGF-β1 and IL-6 expression than rAAV8-transduced muscles (**Supplementary Figure S3**). We also examined humoral immune responses against the rAAV particles in the sera of rAAV-injected dogs. The levels of serum IgG in reaction to rAAV2 or rAAV8 gradually increased with time in both serotypes (**Figure 3b**). These results suggest

Table 1 Summary of gene transduction experiments

Dog ID	Sex	Age[a]	BW[b]	rAAV serotype	Transgene	Route	Muscle	Vector dose[c]	Transgene expression[d]			Cellular infiltration[e]		
									2 weeks	4 weeks	8 weeks	2 weeks	4 weeks	8 weeks
2201MN	M	10	4.5	2	lacZ	i.m.	TA, ECR	1×10^{11}	–	–		–	++	
3004MN	M	5	2.8	2	lacZ	i.m.	TA, ECR	1×10^{11}	±	–		+	±	
3007FN	F	5	2.5	2	lacZ	i.m.	TA, ECR	1×10^{11}	±	±		++	++	
2204FN	F	10	2.5	2	lacZ	i.m.	TA, ECR	1×10^{12}	–	–		+	++	
2801FN	F	10	5.2	2	lacZ	i.m.	TA, ECR	1×10^{12}	+	–		+	++	
2901MN	M	6	2.8	2	lacZ	i.m.	TA, ECR	1×10^{12}	–			±		
7M48	M	7	3.3	2	lacZ	i.m.	TA, ECR	1×10^{12}	–			+		
2206FN	F	10	3.0	2	lacZ	i.m.	TA, ECR	1×10^{13}	±	±		+	++	
2205MN	M	10	4.2	8	lacZ	i.m.	TA, ECR	1×10^{11}	++	±		–	++	
2905MN	M	6	2.8	8	lacZ	i.m.	TA, ECR	1×10^{11}	±			–		
NL52F	F	10	3.5	8	lacZ	i.m.	TA, ECR	1×10^{12}	+++			±		
2106FN	F	6	3.2	8	lacZ	i.m.	TA, ECR	1×10^{12}	+++	–		–	++	
7M49	F	6	3.2	8	lacZ	i.m.	TA, ECR	1×10^{12}		±	–		++	±
2109FMN	M	7	3.3	8	lacZ	i.m.	TA, ECR	1×10^{12}	+++			–		
2903MN	M	6	3.2	8	lacZ	i.m.	TA, ECR	1×10^{12}	+++			±		
2209MN	M	10	4.3	8	lacZ	i.m.	TA, ECR	1×10^{13}	+++	±		±	+++	
2309FA	F	6	3.2	8	M3	i.m.	TA, ECR	1×10^{12}	±	+				
LH49F	F	8	3.3	8	lacZ	i.v.		1×10^{13}	+++			+		
3805MN	M	6	3.5	8	lacZ	i.v.		1×10^{13}		+++	+		+	+
2704FA	F	8	3.6	8	M3	i.v.		1×10^{13}	+	+++				
4001MA	M	6	3.2	8	M3	i.v.		1×10^{13}		+++	+			

BW, body weight; F, female; M, male.
[a]Age at injection (weeks). [b]BW at injection (kg). [c]Vectors (vg/ml) were intramuscularly (i.m.) injected into extensor carpi radiolis (ECR) (1 ml) and tibialis anterior (TA) (2 ml) on both sides. Vectors were also intravenously (i.v.) injected into the lateral saphenous vein (vg/kg/limb) by using limb perfusion method. [d]β-Gal or microdystrophin-positive fibers per 3,000 fibers: –, 0; ±, <100; +, <300; ++, <1,000; +++, >1,000. [e]Infiltrating cells: –, not detected; ±, a few; +, moderate; ++, extensive.

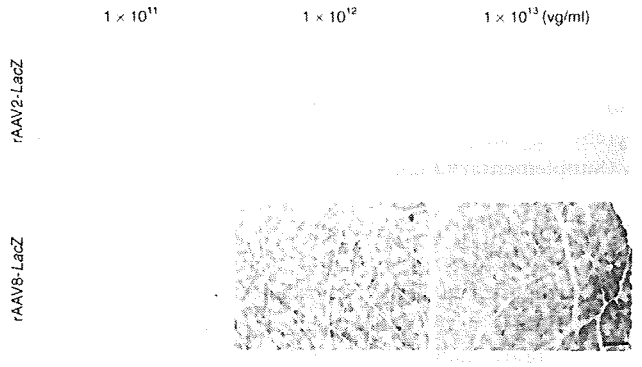

Figure 1 Canine skeletal muscles stained for β-galactosidase. Two milliliters of rAAV2-*lacZ* or rAAV8-*lacZ* (1×10^{11}–10^{13}vg/ml) were injected intramuscularly into the tibialis anterior (TA) muscle of normal dogs ($n = 16$) under ultrasonographic guidance. The muscles were biopsied 2 weeks after the injection. Upper: rAAV2-*lacZ*-injected TA muscles, Lower: rAAV8-*lacZ*-injected TA muscles. Bar = 200 μm.

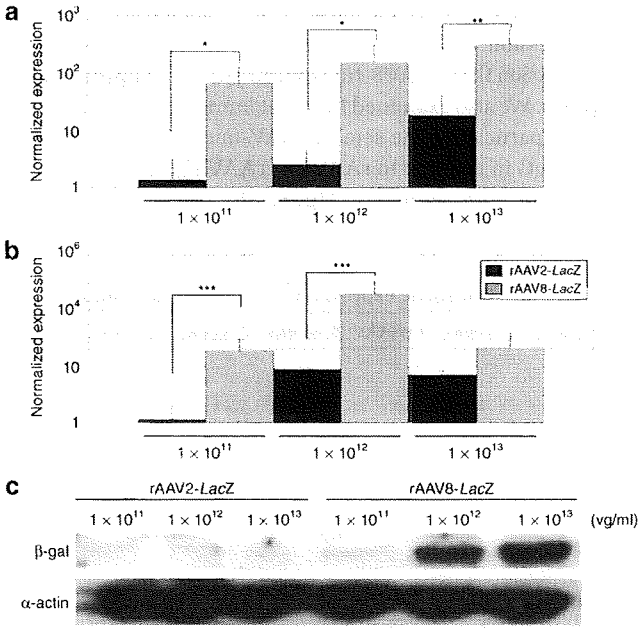

Figure 2 Quantification of viral vector genome, mRNA, and transgene expression. (**a**) Relative quantification of genomic PCR for rAAV2-*lacZ*-injected muscle (black bars) or rAAV8-*lacZ*-injected muscle (gray bars). DNA samples were extracted from the TA muscles. $^{*}P < 0.05$. $^{**}P < 0.01$. Error bars represent 2 SD. (**b**) Relative quantification showed more extensive β-gal mRNA expression caused by rAAV8-*lacZ* (gray bars) as compared to that caused by rAAV2-*lacZ* (black bars). 18S rRNA was used for an internal control. $^{***}P < 0.05$. Error bars represent 2 SD. (**c**) Western blots of β-gal protein (120 kDa) and α-actin (42 kDa); the β-gal signal was normalized to α-actin for comparison.

that cellular and humoral immune responses are elicited in both rAAV2- and rAAV8-transduced muscles.

Bone marrow-derived DC reactions to rAAV2 and rAAV8

We next cultured bone marrow-derived DCs to investigate their response to rAAV injection in dogs. Flow cytometric analyses of these cells at 7 days of culture revealed marked expressions of CD11c and MHC class II molecules on the

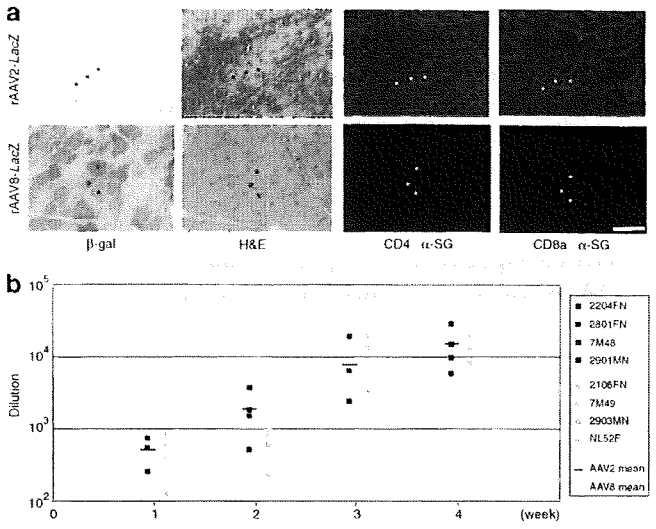

Figure 3 Immune response to rAAV. (**a**) Lymphocyte infiltration after rAAV transduction. Muscles were biopsied 2 weeks after rAAV2- or rAAV8-*lacZ* injection (2×10^{12}vg/muscle). Serial cross-sections were stained with β-gal and H&E, and were immunohistochemically stained with antibodies against canine CD4, CD8a (Alexa 568, red), and α-sarcoglycan (α-SG, Alexa 488, green). Upper: rAAV2-*lacZ*-injected TA muscle; lower: rAAV8-*lacZ*-injected TA muscle. Bar = 100 μm. (**b**) Humoral immune responses to rAAV capsid in dogs. Serum was collected weekly from rAAV2- or rAAV8-*lacZ*-injected dogs and analyzed for the presence of IgG antibody against the rAAV2 or rAAV8 capsid. The data represent dilution rates with 50% reactivity of anti-rAAV2 (black boxes) and anti-rAAV8 (gray boxes) capsid antibodies. The mean reconstitution values are shown as straight lines. Each symbol represents an individual dog that was injected with rAAV at 2×10^{12}vg/muscle.

surface (**Figure 4a,b**). The DCs were cultured with the rAAV-*luciferase* of either serotype 2 or 8 for 48 hours to evaluate transduction efficiency, or cultured with rAAV-*lacZ* for 4 hours to investigate kinetic changes in mRNA. The luciferase assay showed that the transduction efficiency of rAAV2-*luciferase* in DCs was approximately two times that of rAAV8-*luciferase* (**Figure 4c**). mRNA levels of MyD88 and costimulating factors, such as CD80, CD86, and type I interferon (interferon-β, IFN-β) were elevated in both conditions (**Figure 4d**), suggesting that rAAV8 also induces a considerable degree of innate immune response in dog skeletal muscles. Although rAAV2-transduced DCs showed higher IFN-β expression than rAAV8-transduced DCs, the differences between the effects of rAAV2 and rAAV8 on the mRNA levels of MyD88, CD80, CD86, and IFN-β were not statistically significant.

Successful *microdystrophin* gene transfer with rAAV8 into dystrophic dogs

Dystrophin expression in normal skeletal muscle is localized on the sarcolemma, whereas it is totally absent in $CXMD_J$ dogs (**Supplementary Figure S4a,b**). Microdystrophin expression in the rAAV8-injected skeletal muscle of $CXMD_J$ dogs was maintained, even in the absence of any immunosuppressive therapy, for at least 4 weeks after the injection (**Table 1**). Previously, we had shown that microdystrophin expression of ca 20% was sufficient to achieve functional recovery in mdx mice[6]. However, the amount of the expression in intramuscularly injected muscles

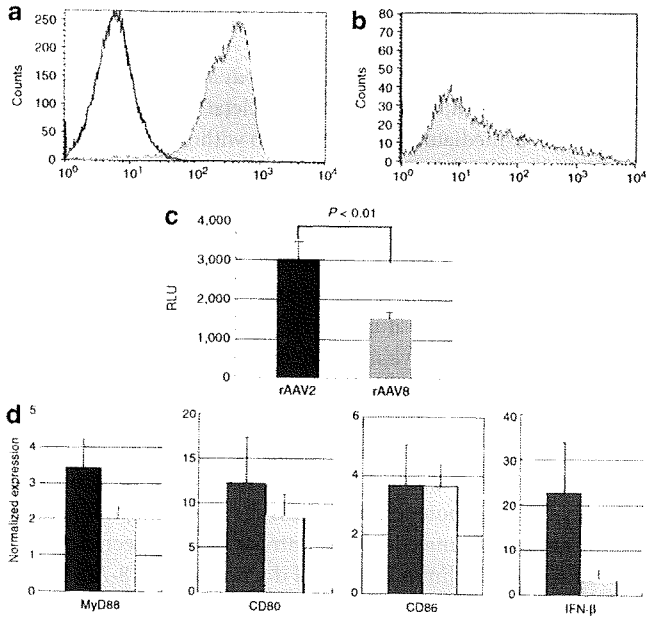

Figure 4 Responses of dendritic cells (DCs) to rAAV in dogs. Bone marrow-derived DCs were obtained from the humerus bones of dogs and cultured in RPMI (10% FCS, p/s) for 7 days with canine GM-CSF and IL-4. (**a**) Flow cytometric analysis of cell surface molecules on day 7. The cells were stained with PE-conjugated CD11c antibody and isotype control. (**b**) DCs were stained with FITC-conjugated MHC Class II antibody and isotype control. (**c**) DCs were transduced with rAAV-*luciferase* (1×10^6vg/cell) for 48 hours. To analyze luciferase expression relating to the use of rAAV2 or rAAV8, relative light unit (RLU) ratios were measured. $^*P < 0.01$. Error bars represent s.e.m., $n = 8$. (**d**) DCs were transduced with 1×10^6vg/cell of rAAV2 (black bars) or rAAV8-*lacZ* (gray bars) for 4 hours, and mRNA levels of MyD88, CD80, CD86, and IFN-β were analyzed. Untransduced cells were used as a control to demonstrate the relative value of expression. The results are representative of two independent experiments. Error bars represent s.e.m., $n = 3$.

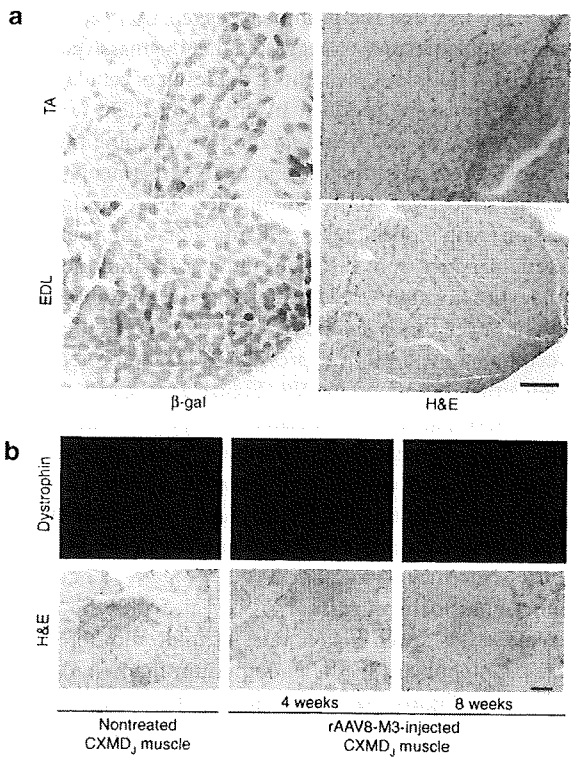

Figure 5 rAAV8-mediated muscle transduction using the limb perfusion method. (**a**) Transduction of normal dog with rAAV8-*lacZ*, using the limb perfusion method. Muscles were biopsied 2 weeks after the injection and stained with β-gal and H&E. TA, tibialis anterior, EDL, extensor digitorum longus. Bar = 200μm. (**b**) Transduction of canine X-linked muscular dystrophy in Japan (CXMD$_J$) dog with rAAV8-*M3*. Muscles of CXMD$_J$ dogs were biopsied 4 and 8 weeks after limb perfusion with rAAV8-*M3*. Samples were immunohistochemically stained with anti-dystrophin antibody (dys2, NCL). Left: nontreated CXMD$_J$ muscle. Middle and right: muscles injected with rAAV-*M3* using limb perfusion method, examined at 4 or 8 weeks after the transduction. Bar = 100μm.

seemed to be insufficient to produce the expected functional recovery (**Supplementary Figure S4c**).

For more efficient gene delivery by rAAV8, we tried a limb perfusion method in the hind limb through the lateral saphenous vein, in an attempt to prevent muscle damage due to direct injection and to bypass immune activation through DCs in the injected muscle. We had observed highly efficient β-gal expression in nearly all the muscles of the distal hind limb at 2 weeks after a single injection (**Table 1**, **Figure 5a**). We then injected rAAV8-*M3* into the hind limbs of CXMD$_J$ dogs, using the same method (**Table 1**). The induction of microdystrophin expression in the muscle at 4 weeks after intravascular injection was more efficient and free of noticeable immune response as compared to intramuscularly injected muscle (**Figure 5b**, **Supplementary Figure S4d**). These results suggest that the intravascular method is superior to the intramuscular method of administration. Although microdystrophin expression persisted at 8 weeks after injection of rAAV8-*M3*, the number of microdystrophin-positive cells at this time point was lower than in the muscles that were sampled at 4 weeks after injection. It is clear, therefore, that long-term microdystrophin expression can be obtained by the limb perfusion method, but that the expression does not last at the same level over a period of weeks. The same phenomenon was observed in rAAV8-*lacZ*-transduced muscles (**Supplementary Figure S5**).

DISCUSSION

In this article, we present evidence that the transfer of rAAV8-*lacZ* to canine skeletal muscles produces higher transgene expression with less lymphocyte proliferation than rAAV2-*lacZ* does, at 2 weeks after injection. Given the advantages of rAAV8, the administration of rAAV8-*M3* by limb perfusion produced extensive transgene expression in the distal limb muscles of CXMD$_J$ dogs without obvious immune responses for as long as 8 weeks after injection. However, transgene expression in the rAAV8-transduced muscles attenuated in the absence of an immunosuppressive regimen over the course of observation. In addition, humoral immune responses were elicited by both rAAV2 and rAAV8. mRNA levels of MyD88 and costimulating factors such as CD80, CD86, and type I interferon (interferon-β) were elevated in both rAAV2- and rAAV8-transduced DCs *in vitro*.

In our previous study, we had demonstrated extensive lymphocyte-mediated immune responses to rAAV2-*lacZ* after direct intramuscular injection into dogs, in contrast to the reported successful delivery of the same viral construct into mouse skeletal

muscle.[8] The fact that the promoter-deleted rAAV2 caused fewer cytotoxic cellular responses suggested that the massive destruction of transduced muscle cells might be the result of cellular immunity against the transgene product. In this study, there was extensive expression of β-gal in rAAV8-*lacZ*-injected canine muscles even in the absence of any immunosuppressive treatments (**Figure 1**), while the rAAV2-*lacZ*-injected muscles showed minimal β-gal expression with considerable inflammatory infiltration. If the transgene product were the main inducer of immune responses, lymphocyte activation would be correlated with transduction efficiency; however, this is not the case based on our results relating to the vector genome, mRNA expression level, and protein delivered through either rAAV2 or rAAV8 (**Figure 2**). These data suggested that the rAAV particle is associated with potent immunogenicity. Besides, β-gal expression disappeared 4 weeks after injection in the rAAV8-injected muscle as in the rAAV2-transduced muscles (**Supplementary Figure S2**). To investigate whether AAV itself has immunogenicity properties, we further characterized the immune responses caused by rAAV2 or rAAV8.

Immunohistochemical analysis revealed that the rAAV2-injected muscles showed higher rates of infiltration of $CD4^+$ and $CD8^+$ T lymphocytes in the endomysium than rAAV8-injected muscles did (**Figure 3a**). Considering the stringent immunogenicity of *lacZ* gene expression, we normalized the activity of TGF-β1 and IL-6 by lacZ expression to exclude the effect of transgene products (**Supplementary Figure S3a**). The total activity of TGF-β1 and IL-6 in the rAAV8-injected muscles was higher than that in rAAV2-injected muscles (**Supplementary Figure S3b**). As a result, rAAV2 induced a stronger cellular immune response than rAAV8 did. To investigate the humoral immune response, we quantitated neutralizing antibodies against rAAV particles in the sera of rAAV-injected dogs (**Figure 3b**). Antibodies against AAV2 and AAV8 capsids were below the detectable level before the injection and were elevated with time after the injection. Because the dogs were bred in a specific pathogen-free facility and not vaccinated, we assume that the elevation of antibody levels was not caused by anamnestic reaction.

Recently, Li *et al.*[10] reported that the AAV2 capsid can induce a cellular immune response through MHC class I antigen presentation with a cross-presentation pathway, and the effects of rAAV2 on human DCs have been described.[10,13] In contrast, other serotypes such as rAAV8 induced less T-cell activation.[11,14] Plasmacytoid DCs are critically important in innate immunity because of their unsurpassed ability to present adenoviral antigens to T-cells for the generation of primary cellular and humoral immune responses.[15–17] The response of DCs against rAAV in dogs was yet to be elucidated. We prepared bone marrow-derived DCs to investigate rAAV-mediated transduction of DCs. The difference between rAAV2 and rAAV8 in respect of the transduction rate of DCs *in vitro* was no greater than the difference in distinct β-gal expressions *in vivo* (**Figure 2,4c**). Quantitative analysis of mRNA of the transduced DCs by RT-PCR revealed that both rAAV2 and rAAV8 upregulated the expression of costimulating factors, with no significant difference between mRNA levels in rAAV2- and rAAV8-transduced cells. Therefore, both rAAV2 and rAAV8 may activate innate immunity in the context of extensive muscle transduction. Whereas AAV capsids cause immune response, transgene products may play adjuvant roles in the immunity to the AAV capsids.[18]

rAAV8 encoding the human *microdystrophin* gene was also intramuscularly injected into the skeletal muscles of $CXMD_J$ dogs. rAAV8-mediated gene expression without any immunosuppression was confirmed over a period of 8 weeks after the injection, whereas there was much less transduction with the use of rAAV2 (data not shown). rAAV8-mediated transduction was also expected to provide effective intravenous delivery.[12] In this context, the venous system is an attractive route for limb perfusion administration because it is a direct channel to multiple muscles of the limb. Moreover, veins are easier to access through the skin and there is less potential for muscle damage during injection. By using the limb perfusion method, we could reach nearly all the muscles of the lower limb, held transiently isolated by a tourniquet around the thigh. Limb perfusion administration could possibly have the potential to bypass the DC recognition caused by intramuscular injection. We intravenously injected rAAV8-*lacZ* into the hind limbs of normal dogs and rAAV8-*M3* into the hind limbs of $CXMD_J$ dogs, and obtained more extensive expression of β-gal or microdystrophin than by intramuscular injection. Interestingly, the inflammatory response was not significant in the intravenously injected muscles, although no immune suppression was attempted. We think that one reason rAAV8-*M3* resulted in better expression than rAAV8-*lacZ* is that the immunogenicity of *M3* is lower than that of *lacZ*. Although microdystrophin expression was lower at 8 weeks after the transduction with the limb perfusion, cellular infiltration was not significant.

In the future, systemic delivery of rAAV8-*microdystrophin* could ameliorate the symptoms of DMD patients. Even though portal vein injection of rAAV2-*FIX* into hemophilia B dogs produced long-term expression, a clinical study failed to demonstrate long-term expression in humans.[19,20] In advance of future clinical trials, several studies are required to confirm safety. Sequential peripheral blood monitoring showed no severe adverse events, including liver dysfunction, during 8 weeks (data not shown). We are now developing a systemic delivery strategy with a muscle-specific promoter. It is also necessary to improve vector constructs or regulate immune reaction against transgene products. Recently, Wang *et al.* reported sustained AAV6-mediated human microdystrophin expression in dystrophic dogs for 30 weeks, using combined immunosuppressive therapy of Ciclosporin, Mycophenolate Mofetil, and anti-thymocyte globulin.[9] In this study with rAAV8-*M3*, we confirmed effective transduction into dog skeletal muscle for 4 weeks without immunosuppressive therapy. However, considering the fact that not only rAAV2 but also rAAV8 induced activation of DCs *in vitro*, immunological modulation would be required for sufficient long-term expression. A novel protocol with systemic or localized immunosuppression using immunosuppressive drugs or local immunosuppression with an IFN-α or -β blockade could help avoid host immune reaction.

In summary, we achieved successful rAAV8-mediated muscle transduction in wild-type dogs as well as in dystrophic dogs by using the limb perfusion method of administration. Also, by manipulating bone marrow-derived DCs, we observed the probable contribution of antigen-presenting cells to the immune response against rAAV8-mediated gene therapy. Although the

cellular responses against rAAV8 were not significant *in vivo*, this DC activation may possibly be involved in limiting long-term transduction when the limb perfusion method is used. The limb perfusion transduction protocol with improved AAV constructs or immune modulation would further enhance rAAV8-mediated transduction strategy and lead to therapeutic benefits.

MATERIALS AND METHODS

Animals. Five- to ten-week-old male and female wild-type dogs obtained from the Beagle-based CXMD$_j$ breeding colony at the National Center of Neurology and Psychiatry (Tokyo, Japan) were used for the *lacZ* gene transduction.[3] Six- to eight-week-old CXMD$_j$ dogs were used for *microdystrophin* gene transduction. All the animals were cared for and treated in accordance with the guidelines approved by the Ethics Committee for Treatment of Laboratory Animals at National Center of Neurology and Psychiatry, where the three fundamental principles of replacement, reduction, and refinement are also considered. Dogs were not vaccinated to avoid the immune responses to vaccination.

Construction of proviral plasmid and recombinant AAV vector production. The AAV2 vector proviral plasmids harboring the *lacZ* or *luciferase* gene with a CMV promoter and SV40 late-gene polyadenylation sequence were propagated.[8] As a therapeutic gene for DMD, the human *microdystrophin* gene, *M3*, was used under the control of the CMV promoter and a bovine growth hormone polyadenylation sequence.[21] The vector genome was packaged into the AAV2 capsid or pseudotyped AAV8 capsid in HEK293 cells. A large-scale cell culture method with an active gassing system was used for transfection.[22] The vector production process involved triple transfection of a proviral plasmid, an AAV helper plasmid pAAV-RC (Stratagene, La Jolla, CA) or p5E18-VD2/8, and an adenovirus helper plasmid pHelper (Stratagene).[21] All the viral particles were purified by CsCl gradient centrifugation. The viral titers were determined by quantitative PCR using SYBR-green detection of PCR products in real time with the MyiQ single-color detection system (Bio-Rad, Hercules, CA) and the following primer sets: for AAV-*lacZ*, lacZ-Q60: forward primer 5′-TTATCAGCCGGAAAACCTACCG-3′, and reverse primer 5′-AGCCAGTTTACCCGCTCTGCTA-3′; for AAV-*microdystrophin*: forward primer 5′-CCAAAAGAAAAAGGATCCACAA-3′, and reverse primer 5′-TTCCAAATCAAACCAAGAGTCA-3′; and for AAV-*luciferase*: forward primer 5′-GATACGCTGCTTTAATGCCTTT-3′, and reverse primer 5′-GTTGCGTCAGCAAACACAGT-3′.

Direct administration of rAAVs into normal and dystrophic skeletal muscle. Experimental dogs (n = 16) were sedated with isoflurane by mask inhalation and intubated. Anesthesia was maintained with 2–4% isoflurane. Two milliliters of rAAV2-*lacZ* or rAAV8-*lacZ* (1×10^{11}–10^{13} vg/ml) were injected intramuscularly into the tibialis anterior muscles and 1 ml into the extensor carpi radialis muscles of the normal dogs under ultrasonographic guidance. rAAV8-*M3* (1×10^{12} vg/ml) was intramuscularly injected at a volume of 2 ml into the tibialis anterior muscles and 1 ml into the extensor carpi radialis muscles of a CXMD$_j$ dog.

Intravenous delivery of rAAVs into the limb veins of dogs. Intravenous injection was administered as described elsewhere.[12] Briefly, a blood pressure cuff was applied just above the knee of an anesthetized normal dog. A 24-gauge intravenous catheter was inserted into the lateral saphenous vein, connected to a three-way stopcock, and flushed with saline. With the blood pressure cuff inflated to over 300 mm Hg, saline (2.6 ml/kg) containing papaverine (0.44 mg/kg, Sigma-Aldrich, St Louis, MO) and heparin (16 U/kg) was injected by hand over 10 seconds. The three-way stopcock was connected to a syringe containing rAAV8-*lacZ* (1×10^{13} vg/kg, 3.8 ml/kg). The syringe was placed in a PHD 2000 syringe pump (Harvard Apparatus, Edenbridge, UK). Five minutes after the papaverine/heparin injection, the rAAV8-*lacZ* was injected at a rate of 0.6 ml/second. Two minutes after the rAAV injection, the blood pressure cuff was released and the catheter was removed. The CXMD$_j$ dogs were injected with rAAV8-*M3* using the same method.

Sampling of transduced muscles. Either the muscles of the transduced dogs were biopsied or the animals were killed at 2, 4, and 8 weeks after the injection. We sampled tibialis anterior and extensor carpi radialis muscles on both sides in the intramusculary transduced dog. In the case of the limb perfusion study, tibialis anterior or extensor digitorum longus muscle of the injected side of the leg was sampled. For biopsy and necropsy, the individual muscle was cropped tendon-to-tendon, divided into several pieces, and immediately frozen in liquid nitrogen-cooled isopentane. Two to eight blocks were sampled from the transduced muscle. We analyzed at least 30 sections from the blocks to observe the general representation.

Histological analysis. Transverse cryosections (10 μm) from the rAAV-*lacZ*-injected muscles were stained with hematoxylin and eosin or 5-bromo-4-chloro-3-indolyl-β-D-galactopyranoside.[24] Eight-micrometer-thick cryosections from the rAAV-*M3*-injected muscles were immunohistochemically stained as described.[24] Briefly, the cryosections were fixed by immersion in cold acetone at −20 °C. Fixed frozen sections were blocked in 5% goat serum in phosphate-buffered saline at room temperature and incubated with mouse monoclonal anti-dystrophin C-terminal antibody (NCL-dys2, Novocastra, Newcastle upon Tyne, UK). The signal was visualized with an Alexa 568-conjugated anti-mouse IgG. Fluorescent signals were observed using a confocal laser scanning microscope (Leica TCS SP, Leica, Heidelberg, Germany). Immunohistochemical analyses were performed with mouse monoclonal antibodies against canine CD4 (CA13.1E4, Serotec, Oxford, UK), canine CD8a (CA9. JD3, Serotec), and double-stained with rabbit polyclonal antibody against α-sarcoglycan.[25] The signal was visualized with an Alexa 568-conjugated anti-mouse IgG, and 488-conjugated anti-rabbit IgG.

Detection of AAV genomes. Total DNA was extracted from muscle cryosections. Cryosections were homogenized using a Multi-beads shocker (Yasui Kikai, Osaka, Japan), and extracted using a Wizard SV Genomic DNA purification system (Promega, Madison, WI). The rAAV genome was detected by relative quantitative PCR using SYBR-green detection of PCR products in real time with a primer set of *lacZ*-Q60. For an internal control, forward primer, 5′-GAACACGCGTTAATAAGGCAATCA-3′, and reverse primer, 5′-CTGACATTCATCGCATCTTTGACA-3′, directed to an ultra-conserved region, were used.[26]

Real-time RT-PCR. Total RNA was isolated from cryosections using a Multi-beads shocker (Yasui Kikai), and RNeasy Fibrous Tissue Mini kit (Qiagen, Hilden, Germany), and first-strand cDNA was synthesized using a QuantiTect Reverse Transcription kit (Qiagen). mRNA was detected using primer sets of lacZ-Q60, forward primer 5′-TGATGGCTA CTGCTTTCCCTAC-3′ and reverse primer 5′-GAGATTTTGCCGA GGATGTACT-3′ for IL-6, and forward primer 5′-CAAGGATCTGGGC TGGAAGTGGA-3′ and reverse primer, 5′-CCAGGACCTTGCTGTA CTGCGGT-3′ for TGF-β1. For an internal control, a primer set of 18S rRNA (Ambion, Foster City, CA) was used.

Western blot analysis. Muscle cryosections were homogenized with four volumes of sample buffer (10% SDS, 70 mmol/l Tris-HCl, 10 mmol/l EDTA, and 5% β-mercaptoethanol). The samples were boiled for 5 minutes and centrifuged at 14,500 rpm for 15 minutes. Protein samples (30 μg per lane) were electrophoresed on a 7.5% polyacrylamide gel (Bio-Rad). The membranes were incubated with a 1:1,000 dilution of the primary antibody for detecting 120 kDa lacZ protein (rabbit anti-β-galactosidase IgG fraction, Molecular Probes, Eugene, OR) or 42 kDa α-actin (mouse anti α-sarcomeric actin IgM, Sigma-Aldrich). Anti-rabbit IgG peroxidase F(ab′)

(GE Healthcare, Buckinghamshire, UK), or peroxidase-conjugated donkey anti-mouse IgM (Jackson ImmunoResearch Laboratories, West Grove, PA) was used for ECL immunodetection (GE Healthcare). Quantification of LacZ protein was performed using a specialized software (ImageJ, US National Institutes of Health, Bethesda, MD).

ELISA for anti-canine AAV IgG. A microtiter plate (MS-8596F, Sumitomo Bakelite, Tokyo, Japan) was precoated with promoter-deleted rAAV2 or rAAV8 (2×10^9 genomes/well) and blocked with a blocking buffer (Block Ace, DS Pharma Biomedical, Osaka, Japan). The plate was incubated for 2 hours at room temperature with the sera from rAAV-transduced dogs, followed by a 1:5,000 dilution of peroxidase-conjugated rabbit anti-dog IgG (Sigma-Aldrich) for 1 hour. Color was visualized using a peroxidase substrate system (TMBZ, ML-1120T, Sumitomo Bakelite). Reactivity was detected at a wave-length of 450 nm with a reference at 570 nm, using an APPLISKAN Multimode Reader (Thermo Fisher Scientific, East Greenbush, NY).

Bone marrow aspiration and preparation of DCs. After the dogs were anesthetized with thiopental and isoflurane, ~0.5 ml of bone marrow was obtained from each humerus by aspiration with a syringe containing 2 ml of 16 mmol/l EDTA-2Na PBS. Bone marrow-derived DCs were generated as described.[15] Mononuclear cells were isolated by density centrifugation using Histopaque-1077 (Sigma-Aldrich). Cells were suspended in RPMI-1640 culture medium (Invitrogen, Carlsbad, CA) supplemented with 10% fetal bovine serum (MP Biomedicals, Aurora, OH) and 1% penicillin-streptomycin (Sigma-Aldrich), and cultured at 37 °C in a humidified 5% CO_2-containing atmosphere. Recombinant canine GM-CSF (25 ng/ml, R&D Systems, Minneapolis, MN) and canine IL-4 (12.5 ng/ml, R&D Systems) were added to the culture medium. On days 3 and 5 of the culture, 60% of the medium volume was changed. On day 7 of the culture, loosely adherent cells were collected and used for fluorescence-activated cell analysis. A FACS Vantage system (Becton Dickinson, Franklin Lakes, NJ) was used for flow cytometry event collection. For the purpose of examining the infectious rate of rAAV, cells were cultured for 48 hours with rAAV2- or 8-*luciferase*. The luciferase activity of rAAV2- or rAAV8-*luciferase* co-cultured cells was estimated using an APPLISKAN Multimode Reader (Thermo Fisher Scientific). Total RNA was isolated using an RNeasy Fibrous Tissue Mini kit (Qiagen), and QuantiTect Reverse Transcription kit (Qiagen). mRNA of cytokines were analyzed using the primer set, forward primer 5′-GAGGAGATGGGCTTCGAGTA-3′ and reverse primer 5′-GTTCCACCAACACGTCGTC-3′ for MyD88; forward primer 5′-GCATCATCCAGGTGAACAAG-3′ and reverse primer 5′-AAGTCAGCAAAGGTGCGATT-3′ for CD80; forward primer 5′-AGGTTACCCAGAACCCAAGG-3′ and reverse primer, 5′-TTGC AGGACACAGAAGATGC-3′ for CD86; and forward primer 5′-ATT GCCTCAAGGACAGGATAAA-3′ and reverse primer 5′-TTGACG TCCTCCAGGATTATCT-3′ for IFN-β. mRNA levels of MyD88, CD80, CD86, and IFN-β in DCs were normalized with a house keeping gene, 18s rRNA. The mRNA levels in the transduced cells were presented as ratios relative to the sample obtained from the untransduced DCs.

Statistical analysis. Statistical significance was determined on the basis of an unpaired, two-tailed Student's *t*-test using specialized software (Statview; SAS Institute, Cary, NC). A *P* value of <0.05 was considered significant.

SUPPLEMENTARY MATERIAL

Figure S1. Histological findings with incisional and nonincisional injection under ultrasonographic guidance.
Figure S2. β-gal expression 4 weeks after injection.
Figure S3. Levels of mRNA were investigated using rAAV-injected muscles.
Figure S4. Intramuscular injection of rAAV8-*M3* into $CXMD_J$
Figure S5. Long-term β-gal expression using limb perfusion injection.
Table S1. Protein expression analyzed with ImageJ.

ACKNOWLEDGMENTS

We thank James M. Wilson for providing pSE18-VD2/8. We also thank Akinori Nakamura, Hiroyuki Nakai, Yuko Nitahara-Kasahara, and Toshimasa Aranami for technical advice and helpful discussions; Kazue Kinoshita for AAV preparation; Ryoko Nakagawa for technical assistance; Satoru Masuda for FACS analysis; and Hideki Kita, Shinichi Ichikawa, and other staff members of JAC Co. for their care of the dogs. This work is supported by Grants-in-Aid for Scientific Research on Nervous and Mental Disorders and Health Sciences Research Grants for Research on Human Genome and Gene Therapy from the Ministry of Health, Labor and Welfare of Japan, and a Grant-in-Aid for Scientific Research from the Ministry of Education, Culture, Sports, Science and Technology (MEXT).

REFERENCES

1. Valentine, BA, Cooper, BJ, de Lahunta, A, O'Quinn, R and Blue, JT (1988). Canine X-linked muscular dystrophy. An animal model of Duchenne muscular dystrophy: clinical studies. *J Neurol Sci* **88**: 69–81.
2. Sharp, NJ, Kornegay, JN, Van Camp, SD, Herbstreith, MH, Secore, SL, Kettle, S *et al.* (1992). An error in dystrophin mRNA processing in golden retriever muscular dystrophy, an animal homologue of Duchenne muscular dystrophy. *Genomics* **13**: 115–121.
3. Shimatsu, Y, Yoshimura, M, Yuasa, K, Urasawa, N, Tomohiro, M, Nakura, M *et al.* (2005). Major clinical and histopathological characteristics of canine X-linked muscular dystrophy in Japan, $CXMD_J$. *Acta Myol* **24**: 145–154.
4. Nakai, H, Fuess, S, Storm, TA, Muramatsu, S, Nara, Y and Kay, MA (2005). Unrestricted hepatocyte transduction with adeno-associated virus serotype 8 vectors in mice. *J Virol* **79**: 214–224.
5. Wang, Z, Zhu, T, Qiao, C, Zhou, L, Wang, B, Zhang, J *et al.* (2005). Adeno-associated virus serotype 8 efficiently delivers genes to muscle and heart. *Nat Biotechnol* **23**: 321–328.
6. Yoshimura, M, Sakamoto, M, Ikemoto, M, Mochizuki, Y, Yuasa, K, Miyagoe-Suzuki, Y *et al.* (2004). AAV vector-mediated microdystrophin expression in a relatively small percentage of mdx myofibers improved the mdx phenotype. *Mol Ther* **10**: 821–828.
7. Gregorevic, P, Allen, JM, Minami, E, Blankinship, MJ, Haraguchi, M, Meuse, L *et al.* (2006). rAAV6-microdystrophin preserves muscle function and extends lifespan in severely dystrophic mice. *Nat Med* **12**: 787–789.
8. Yuasa, K, Yoshimura, M, Urasawa, N, Ohshima, S, Howell, JM, Nakamura, A *et al.* (2007). Injection of a recombinant AAV serotype 2 into canine skeletal muscles evokes strong immune responses against transgene products. *Gene Ther* **14**: 1249–1260.
9. Wang, Z, Kuhr, CS, Allen, JM, Blankinship, M, Gregorevic, P, Chamberlain, JS *et al.* (2007). Sustained AAV-mediated dystrophin expression in a canine model of Duchenne muscular dystrophy with a brief course of immunosuppression. *Mol Ther* **15**: 1160–1166.
10. Li, C, Hirsch, M, Asokan, A, Zeithaml, B, Ma, H, Kafri, T *et al.* (2007). Adeno-associated virus type 2 (AAV2) capsid-specific cytotoxic T lymphocytes eliminate only vector-transduced cells coexpressing the AAV2 capsid *in vivo*. *J Virol* **81**: 7540–7547.
11. Vandenberghe, LH, Wang, L, Somanathan, S, Zhi, Y, Figueredo, J, Calcedo, R *et al.* (2006). Heparin binding directs activation of T cells against adeno-associated virus serotype 2 capsid. *Nat Med* **12**: 967–971.
12. Hagstrom, JE, Hegge, J, Zhang, G, Noble, M, Budker, V, Lewis, DL *et al.* (2004). A facile nonviral method for delivering genes and siRNAs to skeletal muscle of mammalian limbs. *Mol Ther* **10**: 386–398.
13. Zhang, Y, Chirmule, N, Gao, G and Wilson, J (2000). CD40 ligand-dependent activation of cytotoxic T lymphocytes by adeno-associated virus vectors *in vivo*: role of immature dendritic cells. *J Virol* **74**: 8003–8010.
14. Lin, SW, Hensley, SE, Tatsis, N, Lasaro, MO and Ertl, HC (2007). Recombinant adeno-associated virus vectors induce functionally impaired transgene product-specific CD8 T cells in mice. *J Clin Invest* **117**: 3958–3970.
15. Isotani, M, Katsuma, K, Tamura, K, Yamada, M, Yagihara, H, Azakami, D *et al.* (2006). Efficient generation of canine bone marrow-derived dendritic cells. *J Vet Med Sci* **68**: 809–814.
16. Zhu, J, Huang, X and Yang, Y (2007). Innate immune response to adenoviral vectors is mediated by both Toll-like receptor-dependent and -independent pathways. *J Virol* **81**: 3170–3180.
17. Zhang, Z and Wang, FS (2005). Plasmacytoid dendritic cells act as the most competent cell type in linking antiviral innate and adaptive immune responses. *Cell Mol Immunol* **2**: 411–417.
18. Mahadevan, M, Liu, Y, You, C, Luo, R, You, H, Mehta, JL *et al.* (2007). Generation of robust cytotoxic T lymphocytes against prostate specific antigen by transduction of dendritic cells using protein and recombinant adeno-associated virus. *Cancer Immunol Immunother* **56**: 1615–1624.
19. Mount, JD, Herzog, RW, Tillson, DM, Goodman, SA, Robinson, N, McCleland, ML *et al.* (2002). Sustained phenotypic correction of hemophilia B dogs with a factor IX null mutation by liver-directed gene therapy. *Blood* **99**: 2670–2676.

20. Manno, CS, Pierce, GF, Arruda, VR, Glader, B, Ragni, M, Rasko, JJ *et al.* (2006). Successful transduction of liver in hemophilia by AAV-Factor IX and limitations imposed by the host immune response. *Nat Med* **12**: 342–347.
21. Sakamoto, M, Yuasa, K, Yoshimura, M, Yokota, T, Ikemoto, T, Suzuki, M *et al.* (2002). Micro-dystrophin cDNA ameliorates dystrophic phenotypes when introduced into mdx mice as a transgene. *Biochem Biophys Res Commun* **293**: 1265–1272.
22. Okada, T, Nomoto, T, Yoshioka, T, Nonaka-Sarukawa, M, Ito, T, Ogura, T *et al.* (2005). Large-scale production of recombinant viruses by use of a large culture vessel with active gassing. *Hum Gene Ther* **16**: 1212–1218.
23. Ishii, A, Hagiwara, Y, Saito, Y, Yamamoto, K, Yuasa, K, Sato, Y *et al.* (1999). Effective adenovirus-mediated gene expression in adult murine skeletal muscle. *Muscle Nerve* **22**: 592–599.
24. Yuasa, K, Sakamoto, M, Miyagoe-Suzuki, Y, Tanouchi, A, Yamamoto, H, Li, J *et al.* (2002). Adeno-associated virus vector-mediated gene transfer into dystrophin-deficient skeletal muscles evokes enhanced immune response against the transgene product. *Gene Ther* **9**: 1576–1588.
25. Araishi, K, Sasaoka, T, Imamura, M, Noguchi, S, Hama, H, Wakabayashi, E *et al.* (1999). Loss of the sarcoglycan complex and sarcospan leads to muscular dystrophy in beta-sarcoglycan-deficient mice. *Hum Mol Genet* **8**: 1589–1598.
26. Sandelin, A, Bailey, P, Bruce, S, Engstrom, PG, Klos, JM, Wasserman, WW *et al.* (2004). Arrays of ultraconserved non-coding regions span the loci of key developmental genes in vertebrate genomes. *BMC Genomics* **5**: 99.

Acta Myologica • 2008; XXVII; p. 30-36

Vasodilation of intramuscular arterioles under shear stress in dystrophin-deficient skeletal muscle is impaired through decreased nNOS expression

K. Sato[1, 2, 3], T. Yokota[1], S. Ichioka[4], M. Shibata[5], S. Takeda[1]

[1] *Department of Molecular Therapy, National Institute of Neuroscience, National Center of Neurology and Psychiatry, Kodaira, Tokyo 187-8502, Japan;* [2] *Cellport Clinic Yokohama, Minami-nakadori 3-35, Naka-ku, Yokohama, Kanagawa, 231-0006, Japan;* [3] *Department of Plastic and Reconstructive Surgery, Graduate School of Medicine, The University of Tokyo, Bunkyo-ku, Tokyo 113-0033, Japan;* [4] *Department of Plastic and Reconstructive Surgery, Saitama Medical School, Moroyama, Iruma-gun, Saitama 350-0451, Japan;* [5] *Department of Biomedical Engineering, Graduate School of Medicine, The University of Tokyo, Bunkyo-ku, Tokyo 113-0033, Japan*

Duchenne muscular dystrophy (DMD) is a lethal X-linked disorder of striated muscle caused by the absence of dystrophin. Recently, impairment of vascular dilation under shear stress has been found in DMD, but the underlying molecular mechanism is not fully understood. Moreover, dilation of intramuscular arterioles, which may be a key to the molecular pathogenesis, has not been addressed yet. We examined dilation of arterioles in the mouse cremaster muscle under shear stress due to ligation. The vasodilation was significantly impaired in dystrophin-deficient *mdx* mice as well as in neuronal nitric oxide synthase (nNOS)-deficient mice; however, neither endothelial NOS-deficient mice nor α1-syntrophin-deficient mice showed any difference in vasodilation from control mice. These results indicate that nNOS is the main supplier of nitric oxide in shear stress-induced vasodilation in skeletal muscle, but that the sarcolemmal localization of nNOS is not indispensable for the function. In contrast, the response to acetylcholine or sodium nitroprusside was not impaired in *mdx* or nNOS-deficient mice, suggesting that pharmacological treatment using a vasoactive agent may ameliorate skeletal and cardiac muscle symptoms of DMD.

Key words: Duchenne muscular dystrophy, blood flow, dystrophin, nitric oxide synthase, vasodilation

Introduction

Nitric oxide (NO) is a vasoactive agent generated by nitric oxide synthase (NOS). Neuronal NOS (nNOS) is highly expressed in skeletal muscle compared with endothelial NOS (eNOS) and inducible NOS (iNOS). nNOS is anchored by α1-syntrophin, a member of the dystrophin-glycoprotein complex (DGC), at the sarcolemma in skeletal muscle (1-6). Dystrophin is a cytoskeletal protein, and its absence together with the secondary loss of DGC from the sarcolemma is responsible for Duchenne muscular dystrophy (DMD), a severe muscle disease characterized by progressive skeletal muscle degeneration complicated with cardiomyopathy (5). nNOS expression is greatly reduced at the mRNA level in dystrophin-deficient muscle (2). Moreover, the attenuation of α-adrenergic vasoconstriction is impaired in contracting dystrophin-deficient muscle, suggesting that nNOS has a specific role in protection from sympathetic vasoconstriction (7, 8). In addition, the localization of nNOS at the sarcolemma through α1-syntrophin is indispensable for the attenuation of α-adrenergic vasoconstriction during muscle contraction (9). Recently, Loufrani et al. showed that the carotid and mesenteric arteries of *mdx* mice, an animal model of DMD, do not dilate properly under shear stress, although they are dilated normally by treatment with either an NOS stimulator, such as acetylcholine (ACh), or an NO donor, such as sodium nitroprusside (SNP) (10). They concluded that the endothelial dystrophin plays an invaluable role in vasodilation under shear stress. In addition, the molecular background is not clearly understood, although flow-induced remodeling in arterial wall is deficient in *mdx* mice when stimulated by arterial ligation or hydralazine (11, 12). To clarify the role of nNOS in intramuscular arterioles in vivo, we studied vasodilation in the mouse cremaster muscle. We caused the modified parallel occlusion of arterioles by microsurgical nylon thread ligation (13-16). We enlisted the participation of DGC in shear-stress vasodilation by using *mdx* mice. We also determined the significance of the localization of nNOS at the sarcolemma by using α1-

Address for correspondence: S. Takeda, Department of Molecular Therapy, National Institute of Neuroscience, National Center of Neurology and Psychiatry, 4-1-1 Ogawa-higashi, Kodaira, Tokyo 187-8502, Japan. Fax +81 42 3461750. E-mail: takeda@ncnp.go.jp

syntrophin knockout mice (α1syn$^{-/-}$). In addition, we used nNOS knockout (nNOS$^{-/-}$) and eNOS knockout (eNOS$^{-/-}$) mice to clarify which NOS is involved in vasodilation under shear stress.

Materials and methods

Animals

Mdx mice and their controls, C57Bl/10 mice (B10), α1syn$^{-/-}$ mice generated in C57Bl/6 mice (B6), and their wild-type littermates (α1syn$^{+/+}$), aged 8-10 weeks were used (17). Eight- to 10-week-old nNOS$^{-/-}$ and eNOS$^{-/-}$ mice (B6 background) were supplied by the Jackson Laboratory. They were anesthetized by intraperitoneal injection of 1.2×10^{-3} g carbamic acid ethyl ester per gram of body weight. At the end of the experiment, animals were sacrificed by an overdose of pentobarbital. All protocols were approved by the Institutional Animal Care and Use Committee of the National Institute of Neuroscience and were performed in compliance with the Guide for the Care and Use of Division of Laboratory Animal Resources.

Experimental Design

We mounted and fixed mouse on experimental stage under anesthesia and scrotum of each mouse was placed on a clear silicone dish as shown in Figure 1a. The cremaster muscle was exposed as described with minor modification (18), and was observed under an intravital microscope at 450 magnifications. The exposed cremaster muscle was deoxygenated by continuous superfusion (5 ml/min) of buffered Tyrode solution (34 ± 0.5 °C, pH 7.35-7.45) bubbled with 95% N_2 and 5% CO_2 gas. Captured microcirculatory images were converted to digital images by the computer and recorded by VTR (Fig. 1a). To calculate the shear stress, we used CapiFlow® (IM-Capiflow, Kista, Sweden), a fully computerized system for the measurement of red blood cell velocity, as previously described (19, 20).

Drug treatment

We first examined the vasodilatory response of third-order arterioles (A3; about 20 μm) in mouse cremaster muscles (Fig. 1b) (22). ACh or SNP was added to the buffer solution and applied directly to the muscle, based on previous reports with modification (23, 24). The vessel diameter was measured before and just after drug administration and the dilatory ratio was calculated as: diameter of arteriole after drug treatment/ before drug treatment. To determine adequate dose, ACh or SNP was exposed from its lower concentration to higher concentration. Before increasing dose, we waited for maximum ten minutes until no more dilatory effect was observed by previous dose. Papaverin was added at the final part of experiments to know the extent of maximum dilation of vessels. We also examined the effect of NO synthesis inhibition by adding N-omega-nitro-L-arginine methyl ester (L-NAME, 0.1 mmol/L) to the buffer from 10 minutes before ACh or SNP administration.

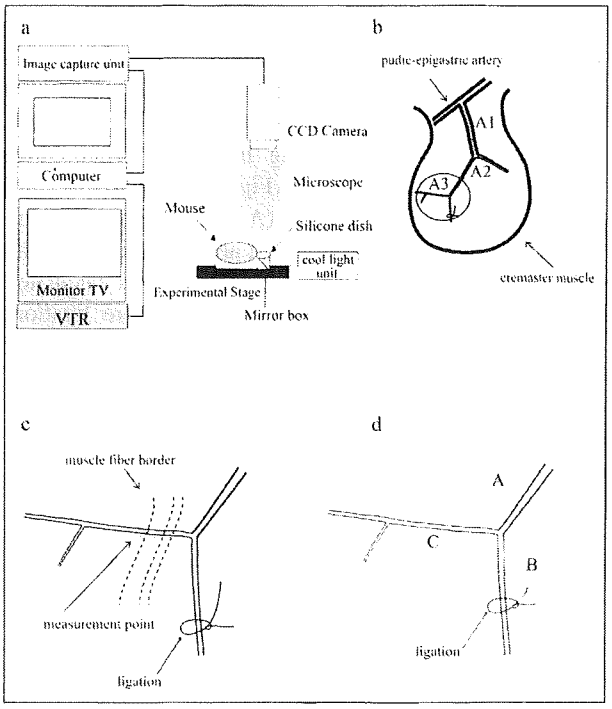

Figure 1. Observation and measurement of dilation of intramuscular arterioles induced by drug treatment or by shear stress in mouse cremaster muscle. (a) Optical system consisting of a cool light unit, mirror box, 450X intravital microscope (MZFL3, Leica Microsystems, Heidelberg, Germany), cooled, color 3 charge-coupled device (CCD) camera, image capture unit (C5810, Hamamatsu Photonics K.K., Hamamatsu, Japan), computer (Apple Macintosh G4, Apple, Cupertino, California), and video cassette recorder (HR-STG300, Victor JVC, Yokohama, JAPAN). (b) Arterioles in the mouse cremaster muscle are classified as indicated. A1; first-order arterioles, A2; second-order arterioles, A3; third-order arterioles. Observation area was indicated by circle. (c) Measurements of arteriole diameter were performed 120-1000 μm from the point of divergence, and the observation point was decided in reference to the border of muscle fibers. (d). Points for measurements of tissue pO_2 during parallel occlusion in A3 area: A, around the main arteriole; B, around the ligation site; and C, the original point for measurements of dilation of arterioles.

Shear stress

We used parallel occlusion method to increase the blood flow velocity in nonoccluded parallel arteriolar branches in vivo, based on the previous studies (13-16). The arteriole was ligated using 10-0 nylon thread with needle to produce shear stress (Fig. 1c) (13). The ligated portion and the measured point (A3) were remote enough from the branching point to avoid artifactual effects. The dilatory ratio for shear stress experiments was calculated as: diameter of arteriole after ligation/ before ligation. The dilatory ratio was also examined under indomethacin ($1.0x10^{-3}$, $5.0x10^{-2}$, $1.0x10^{-2}$ or 0.5 mmol/L) administration, when Prostaglandin I_2 (PGI_2) ($1.0x10^{-4}$ mmol/L) was added to the buffer solution or we induced vasodilation by parallel occlusion. L-NAME and indomethacin were supplied from 10 minutes before ligation. Without L-NAME treatment, shear stress-induced vasodilation was observed for a longer period as long as 20 minutes in 4 B10 and 4 *mdx* mice.

Measurements of partial pressure of oxygen (pO_2)

Observations of the microcirculation and in vivo partial pressure of oxygen (pO_2) measurements were made with a microscope and the oxygen-dependent quenching of phosphorescence decay technique, as previously described (21). We measured tissue pO_2 of B10 (n = 3) and *mdx* mice (n = 3) at three distinct points of cremaster muscles before and after ligation by the phosphorescence quenching method (Fig. 1d).

Histological analysis and immunohistochemistry

Ten-micrometer cryosections of cremaster muscles were prepared, air-dried, and stained with hematoxylin and eosin (H&E). Six-micrometer acetone-fixed cryosections were prepared, blocked with goat serum, and then incubated with primary antibodies, rabbit against nNOS (Zymed Laboratories) and rat against CD31/PECAM-1 (Southern Biotechnology Associates) at room air temperature. Alexa 488-labeled goat anti-rabbit IgG (H + L) (Molecular Probes) and Alexa 594-labeled goat anti-rat IgG (H + L) were used as the secondary antibody. The sections were viewed and photographed by a laser microscope, TCSSP™ (Leica Microsystems).

Statistical analysis

Results were expressed as means ± standard error of the mean (SEM). Results were compared between *mdx* mice and B10, α1syn$^{-/-}$ and α1syn$^{+/+}$ mice, and eNOS$^{-/-}$ or nNOS$^{-/-}$ mice and B6. The effect of L-NAME pretreatment was also evaluated. The significance of the differences between groups was determined by Mann-Whitney U test or ANOVA. Values of $p < 0.05$ were considered to be significant.

Results

Drug induced vasodilation

Maximum arteriolar dilation was determined for administration of ACh or SNP, and then compared with the dilation by the treatment with 1.0 mmol/L of Papaverine. The optimal dose of both ACh and SNP was 1.0 mmol/L for maximum dilatory ratio (Fig. 2) and the dose was used for subsequent examinations (Fig. 3).

The administration of ACh or SNP gave almost the same dilatory ratio between B10 (n = 7) and *mdx* mice (n = 7), α1syn$^{+/+}$ (n = 5) and α1syn$^{-/-}$ (n = 5) and, eNOS$^{-/-}$ (n = 4) or nNOS$^{-/-}$ mice (n = 4) and B6 (n = 4) (Figs. 3a and 3b). This result does not conflict with the conclusion of a previous study using nNOS- and eNOS-deficient mice that expression of either nNOS or eNOS is sufficient for ACh-induced dilation (25). Pretreatment of L-NAME gave the same degree of inhibition in ACh-induced vasodilation in B10 (n = 5) and in *mdx* mice (n = 5), but did not significantly alter the dilatory ratio in SNP-induced vasodilation in these mice.

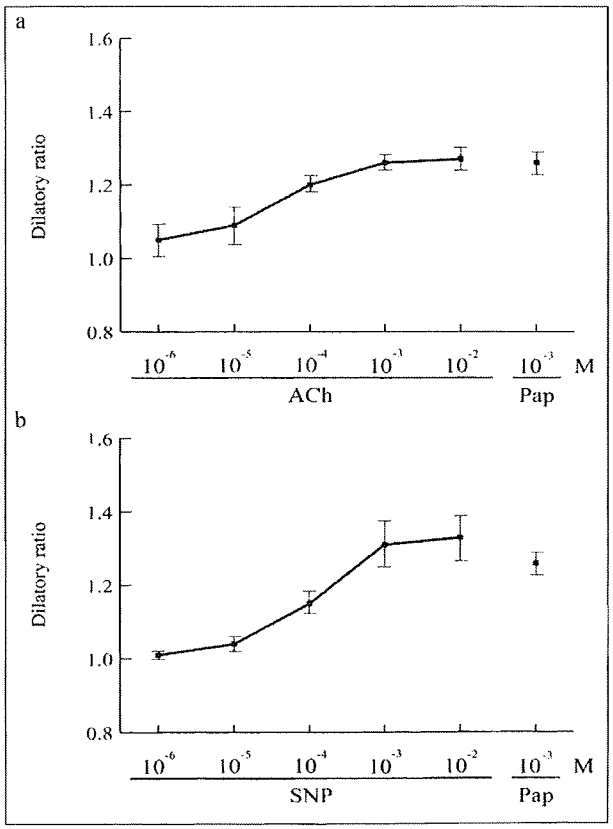

Figure 2. Responses of arterioles for vasodilatory agents, ACh and SNP in three B10. Graphs are showing dilatory ratio against various doses of ACh (a) or SNP (b), in reference to maximum dilation by treatment of 10^{-3} M of Papaverin (Pap).

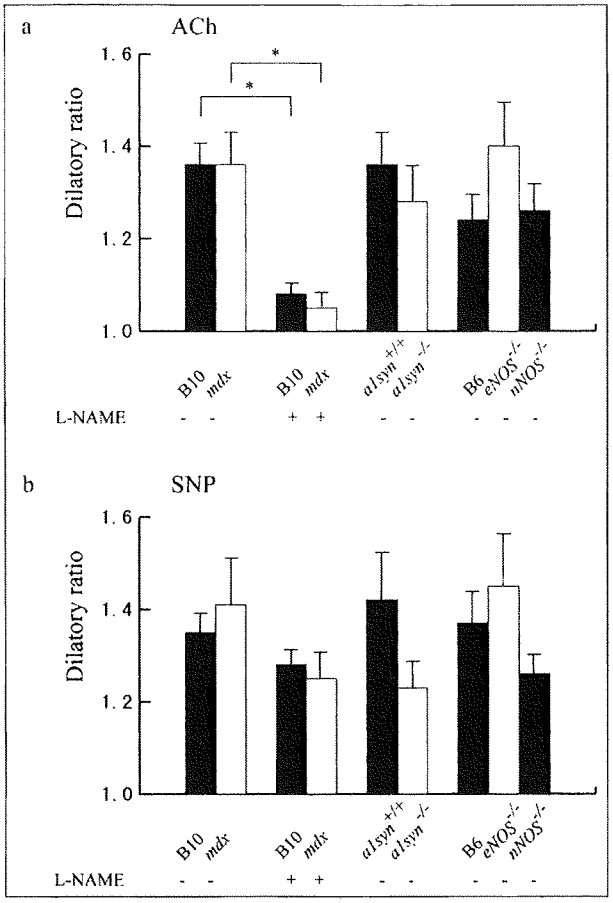

Figure 3. Effects of vasodilative agents on dilation of mouse cremaster arterioles of B10 (black bar), mdx (white bar), B10 pretreated with L-NAME (black bar), mdx pretreated with L-NAME (white bar), $\alpha 1syn^{+/+}$ (black bar), $\alpha 1syn^{-/-}$ (white bar), B6 (black bar), $eNOS^{-/-}$ (white bar), and $nNOS^{-/-}$ (black bar) mice. (a) After pretreatment with L-NAME, ACh-induced vasodilation was reduced both in B10 and in mdx mice. Values are indicated as mean ± SEM. Asterisk (*) shows statistical significance ($p < 0.05$). (b) Vasodilation induced by SNP was not statistically significant between the mice we examined.

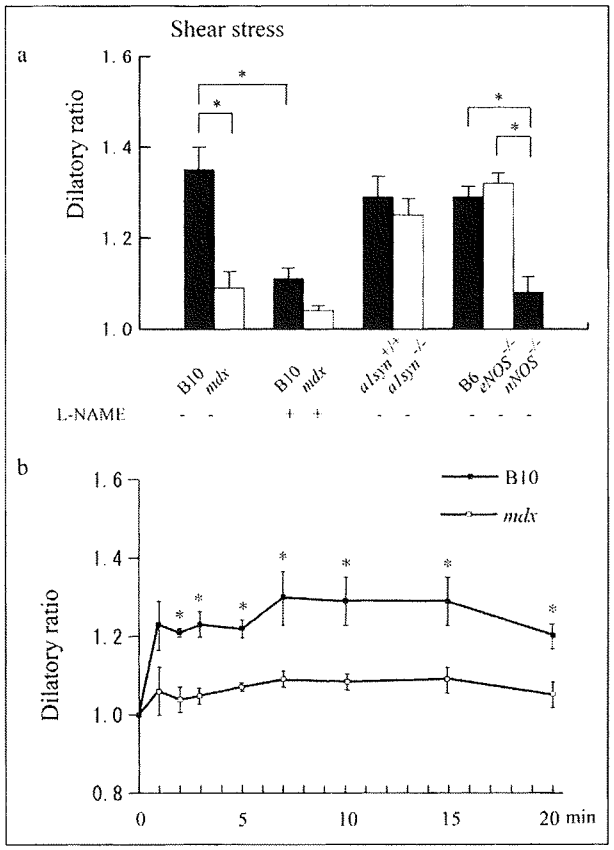

Figure 4. Effects of shear stress-induced dilation of mouse cremaster arterioles of B10 (black bar), mdx (white bar), B10 pretreated with L-NAME (black bar), mdx pretreated with L-NAME (white bar), $\alpha 1syn^{+/+}$ (black bar), $\alpha 1syn^{-/-}$ (white bar), B6 (black bar), $eNOS^{-/-}$ (white bar), and $nNOS^{-/-}$ (black bar) mice. (a) mdx mice, B10 pretreated with L-NAME, mdx mice pretreated with L-NAME and $nNOS^{-/-}$ mice showed impaired vasodilation under shear stress. (b) Extended observation of shear stress-induced vasodilation. The vessel diameter in B10 rapidly increased after vessel ligation and reached a stable level within 10 minutes (n = 4). The dilation of arterioles was severely impaired in mdx mice (n = 4). The difference between mdx mice and B10 was observed as long as 20 minutes after the ligation.

Shear stress-induced vasodilation

In contrast, shear stress-induced vasodilation was significantly impaired in *mdx* mice (n = 10) compared with that of B10 (n = 10) (Fig. 4a), and in addition, the calculated shear stresses were different (Table 1). Interestingly, although $nNOS^{-/-}$ mice (n = 5) showed impaired vasodilation, $eNOS^{-/-}$ mice (n = 5) did not show significant differences in the dilatory ratio when compared with that of B6 (n = 5), indicating that nNOS is the main supplier of NO in the shear stress-induced vasodilation of arterioles in skeletal muscle. On the other hand, $\alpha 1syn^{-/-}$ mice (n = 5) did not show significant differences in the dilation compared with the control $\alpha 1syn^{+/+}$ mice (n = 5), suggesting that the intramuscular localization of nNOS at the sarcolemma is not critical for shear stress-induced vasodilation. After pre-treatment with L-NAME, shear stress-induced vasodilation was significantly decreased in B10 (n = 5).

As shown in Figure 4b, under a longer observation of shear stress-induced vasodilation in the absence of L-NAME, the difference between *mdx* mice and B10 was still observed at least 20 minutes after the ligation.

Table 1. Relationship of vasodilation and shear stress in mouse cremaster arterioles.

	Blood cell velocity (cm/s)		Diameter (μm)		Shear stress rate
	before ligation	after ligation	before ligation	after ligation	
B10 (n = 3)	0.48 ± 0.05	0.67 ± 0.20	18.7 ± 0.9	24.2 ± 0.2	1.02 ± 0.16
mdx (n = 3)	0.41 ± 0.05	0.91 ± 0.23*	18.8 ± 0.7	19.8 ± 0.1*	2.02 ± 0.23*

Shear stress rates were calculated as (shear stress before ligation) / (shear stress after ligation). Values are expressed as mean ± S.E.M. * = $p < 0.05$

PGI_2 induced vasodilation

There were significant differences between shear stress-induced and PGI_2-induced vasodilation in dilatory ratios against high concentrations of indomethacin in B10 (Fig. 5). These data indicated that high concentration of indomethacin treatment could completely antagonize PGI_2-induced vasodilation, but the treatment cannot completely inhibit shear stress-induced vasodilation.

Alternation of pO_2 before and after ligation

There were no significant differences in tissue pO_2 levels between before and after ligation not only in B10 but also in *mdx* mice (Fig. 6).

Immunohistochemical observation of NOS expression

In H&E stained tissues, centrally nucleated fibers, which represent muscle regeneration, were observed in only *mdx* mice (Figs. 7a-c). The immunohistochemical analysis showed that nNOS was observed mainly at the sarcolemma rather than in the endothelium and vascular smooth muscle in B10 and $eNOS^{-/-}$ mice (Figs. 7b and 7h). In $\alpha 1syn^{-/-}$ mice, nNOS was not localized at the sarcolemma but remained in the cytoplasm (Fig. 7f), as previously reported (14, 26). Less nNOS was found in *mdx* mice, and it was not detected in $nNOS^{-/-}$ mice (Figs. 7d and 7j).

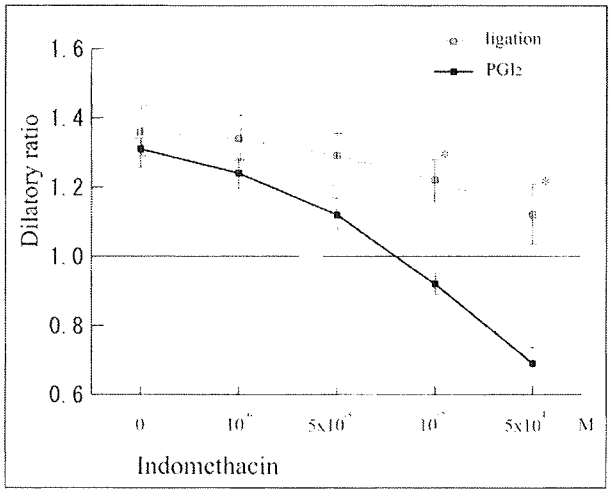

Figure 5. Under various dose of indomethacin, vasodilation was induced either by treatment of Prostaglandin I_2 (PGI_2) or by parallel occlusion (ligation) in B10 cremaster muscle arterioles (n = 5).

Discussion

Nitric oxide is one of the most important factors in shear stress-induced vasodilation especially by parallel occlusion method (10, 14, 27). Other factors, such as prostaglandins, were reported to contribute to shear stress-induced dilation in various models (15, 16, 28), but we showed that indomethacin, an inhibitor of prostaglandins, did not prevent the increase in diameter in shear stress condition. In addition, we concluded that the parallel occlusion method did not cause tissue hypoxia or acute ischemia. Thus, we demonstrated that dilation of arterioles in the mouse cremaster muscle under shear stress by the parallel occlusion method depends mainly on NO, especially that produced by nNOS. In particular, *mdx* and $nNOS^{-/-}$ mice showed impaired vasodilation in parallel occlusion,

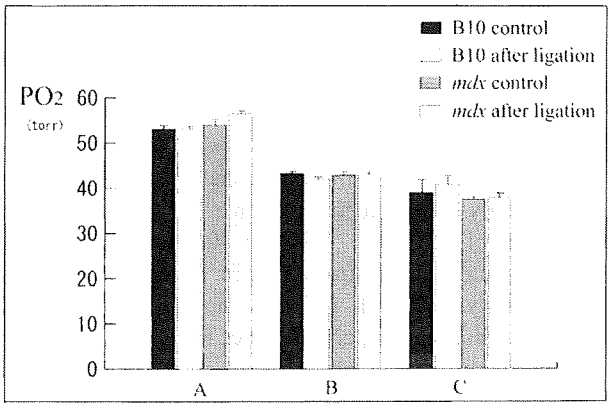

Figure 6. Histogram showing pO_2 at the observation points. There are no significant differences in alterations of tissue pO_2 during parallel occlusion.

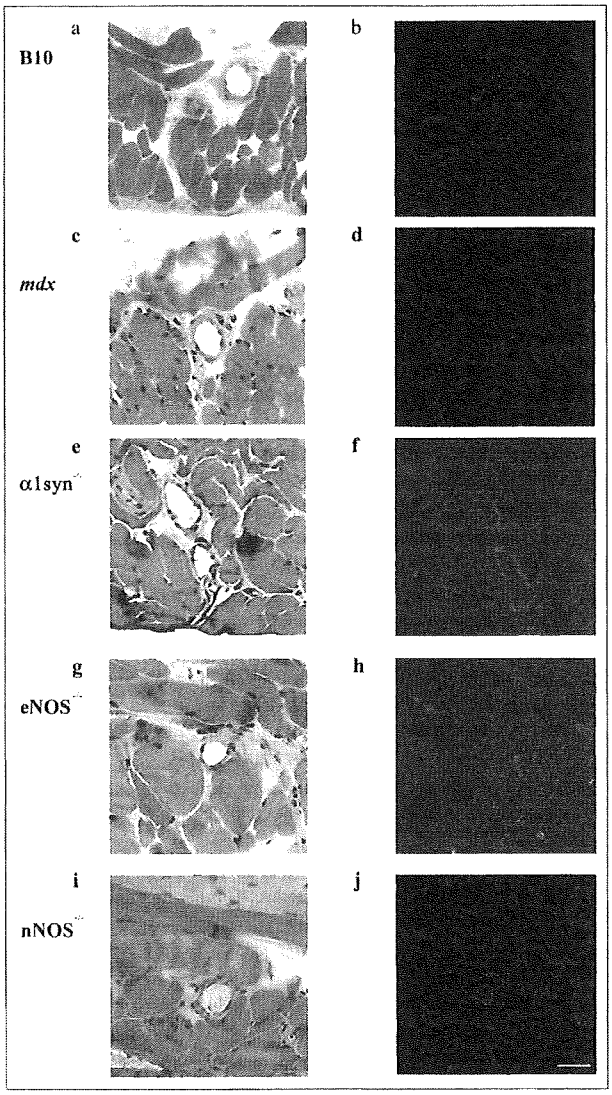

Figure 7. nNOS expression and localization in vascular endothelium and cremaster muscles of mice. H&E (a, c, e, g, and i) and double staining with nNOS (green) and PECAM-1 (red) antibodies (b, d, f, h, and i) of B10 (a, b), mdx (c, d), α1syn$^{-/-}$ (e, f), eNOS$^{-/-}$ (g, h), and nNOS$^{-/-}$ (i, j) mice. Centrally located nuclei, a typical feature of regenerated muscle, are found only in mdx mice (c). In B10 and eNOS$^{-/-}$ cremaster muscles, nNOS expression was observed at the sarcolemma. In contrast, the expression was greatly reduced or not detected in mdx or nNOS$^{-/-}$ mice, respectively. Bar, 40 μm.

whereas responses to ACh and SNP were unaltered. Decreased expression of nNOS in *mdx* skeletal muscle may be important as a cause of this finding.

It is intriguing to know the relationship between shear stress-induced vasodilation and the localization of nNOS. Koller et al. showed that shear stress-induced vasodilation of 80- to 156-μm arterioles was inhibited by removal of the endothelium or by addition of indomethacin in rat cremaster muscle, but they did not identify the responsible molecules of vascular dilation (29). In our study, nNOS expression was mainly found in the sarcolemma and less frequently in the endothelium or vascular smooth muscle, implying that skeletal muscle nNOS is possibly involved in dilation of intramuscular arterioles at the very end of the skeletal muscle circulation under shear stress. nNOS is anchored to the sarcolemma through α1-syntrophin. α1syn$^{-/-}$ mice showed altered distribution of nNOS expression in cytoplasm, but showed no significant differences in shear stress-induced vasodilation between α1syn$^{-/-}$ mice and α1syn$^{+/+}$ mice. Thus, the sarcolemmal localization of nNOS through expression of α1-syntrophin is not indispensable for vasodilation. However, how dystrophin or other molecules transduce mechanostress to soluble nNOS is unresolved (6). The defective vasodilation under shear stress due to nNOS deficiency in *mdx* mice might be related to its muscle degradation (14).

It is very interesting to note the amelioration of dystrophic phenotypes in nNOS transgenic *mdx* mice, although the localization of nNOS cannot have been improved (30). Decreased vasodilation just after muscle contraction has also been demonstrated in *mdx* skeletal muscle (31). Leinonen et al. found that capillary circulation in skeletal muscle was impaired in DMD (32), and deteriorated attenuation of α-adrenergic vasoconstriction during exercise may participate in this pathophysiology (7). Moreover, blood flow must be increased to accommodate the augmented metabolic demands of the muscle, not only in exercise. Intramuscular arterioles in *mdx* mice cannot afford to respond to the increased demands, and their failure may result in relative ischemia in the skeletal muscle and cardiac phenotypes of dystrophin deficiency. Asai et al. very recently showed that the functional ischemia in contraction-induced myofibers in *mdx* mice is due to nNOS deficiency and indicated that vasoactive drugs may ameliorate muscle damage (33). Even in dystrophin-deficient skeletal muscle, cholinergic vascular modulation was well preserved. Therefore, our study indicates that pharmacological treatment using a vasoactive agent is applicable to at least skeletal muscle symptoms in patients suffering from DMD.

In conclusion, we demonstrated that vasodilation of intramuscular arterioles under shear stress was impaired in dystrophin-deficient *mdx* mice. This impairment may be related to phenotypes of DMD, not only in skeletal muscle but also in cardiac muscle.

Acknowledgements

This work was supported by Grants-in-Aid from the Human Frontier Science Program, Scientific Research for

Center of Excellence, Research on Nervous and Mental Disorders (10B-1, 13B-1), Health Science Research Grants for Research on the Human Genome and Gene Therapy (H10-genome-015, H13-genome-001) and for Research on Brain Science (H12-brain-028) from the Ministry of Health, Labor, and Welfare of Japan, Grants-in-Aid for Scientific Research (10557065, 11470153, 11170264, 14657158, and 15390281) from the Ministry of Education, Culture, Sports, Science, and Technology for Japan, and a Research Grant from the Human Frontier Science Project. This work was also carried out as a part of the "Ground-based Research Announcement for Space Utilization" promoted by the Japan Space Forum. T. Yokota is a Research Fellow of the Japan Society for the Promotion of Science (JSPS).

References

1. Brenman JE, Chao DS, Xia H, et al. Nitric oxide synthase complexed with dystrophin and absent from skeletal muscle sarcolemma in Duchenne muscular dystrophy. Cell 1995;82:743-52.
2. Chang W, Iannaccone ST, Lau KS, et al. Neuronal nitric oxide synthase and dystrophin-deficient muscular dystrophy. Proc Nat Acad Sci USA 1996;93:9142-7.
3. Brenman JE, Chao DS, Gee SH, et al. Interaction of nitric oxide synthase with the postsynaptic density protein PSD-95 and α1-syntrophin mediated by PDZ domains. Cell 1996;84:757-67.
4. Yokota T, Miyagoe Y, Hosaka Y, et al. Aquaporin-4 is absent at the sarcolemma and at perivascular astrocyte endfeet in α1-syntrophin knockout mice. Proc Japan Acad 2000;76B:22-7.
5. Hoffman EP, Brown RH Jr, Kunkel LM. Dystrophin: the protein product of the Duchenne muscular dystrophy locus. Cell 1987;51:919-28.
6. Suzuki N, Motohashi N, Uezumi A, et al. NO production results in suspension induced muscle atrophy through dislocation of neuronal NOS. J Clin Invest 2007;117:2468-76.
7. Thomas GD, Sander M, Lau KS, et al. Impaired metabolic modulation of α-adrenergic vasoconstriction in dystrophin-deficient skeletal muscle. Proc Natl Acad Sci USA 1998;95:15090-5.
8. Fadel PJ, Zhao W, Thomas GD. Impaired vasomodulation is associated with reduced neuronal nitric oxide synthase in skeletal muscle of ovariectomized rats. J Physiol 2003;549:243-53.
9. Thomas GD, Shaul PW, Yuhanna IS, et al. Vasomodulation by skeletal muscle-derived nitric oxide requires α-syntrophin-mediated sarcolemmal localization of neuronal nitric oxide synthase. Circ Res 2003;92:554-60.
10. Loufrani L, Matrougui K, Gorny D, et al. Flow (shear stress)-induced endothelium-dependent dilation is altered in mice lacking the gene encoding for dystrophin. Circulation 2001;103:864-70.
11. Loufrani L, Li Z, Levy BI, et al. Excessive microvascular adaptation to chronic changes in blood flow in mice lacking the gene encoding for desmin. Arterioscler Thromb Vasc Biol 2002;22:1579-84.
12. Loufrani L, Henrion D. Vasodilator treatment with hydralazine increases blood flow in *mdx* mice resistance arteries without vascular wall remodeling or endothelium function improvement. J Hyperten 2005;23:1855-60.
13. Koller A, Kaley G. Flow velocity-dependent regulation of microvascular resistance in vivo. Microcirc Endothelium Lymphatics 1989;6:519-29.
14. Koller A, Kaley G. Endothelium regulates skeletal muscle microcirculation by a blood flow velocity-sensing mechanism. Am J Physiol 1990;258:H862-8.
15. Koller A, Kaley G. Prostaglandins mediate arteriolar dilation to increased blood flow velocity in skeletal muscle microcirculation. Circ Res 1990;67:529-34.
16. Frisbee JC, Stepp DW. Impaired NO-dependent dilation of skeletal muscle arterioles in hypertensive diabetic obese Zucker rats. Am J Physio. Heart Circ Physiol 2001;281:H1304-11.
17. Kameya S, Miyagoe Y, Nonaka I, et al. α1-Syntrophin gene disruption results in the absence of neuronal-type nitric-oxide synthase at the sarcolemma but does not induce muscle degeneration. J Biol Chem 1999;274:2193-200.
18. Baez S. An open cremaster muscle preparation for the study of blood vessels in vivo. Microscopy Microvasc Res 1973;5:384-94.
19. Fagrell B, Rosen L, Eriksson SE. Computerized data analysis of capillary blood cell velocity in humans. Int J Microcirc Clin Exp 1994;14:133-8.
20. Bongard O, Fagrell B. Discrepancies between total and nutritional skin microcirculation in patients with peripheral arterial occlusive disease (PAOD). Vasa 1999;19:105-11.
21. Shibata M, Ichioka S, Ando J, et al. Microvascular and interstitial PO(2) measurements in rat skeletal muscle by phosphorescence quenching. Appl Physiol 2001;91:321-7.
22. Kaul DK, Fabry ME, Costantini F, et al. In vivo demonstration of red cell-endothelial interaction, sickling and altered microvascular response to oxygen in the sickle transgenic mouse. J Clin Invest 1995;96:2845-53.
23. Ichioka S, Shibata M, Kosaki K, et al. Effects of shear stress on wound-healing angiogenesis in the rabbit ear chamber. J Surg Res 1997;72:29-35.
24. Ichioka S, Nakatsuka T, Ohura N, et al. Topical application of amrinone (a selective phosphodiesterase III inhibitor) for relief of vasospasm. J Surg Res 2000;93:149-55.
25. Meng W, Ayala C, Waeber C, et al. Neuronal NOS-cGMP-dependent ACh-induced relaxation in pial arterioles of endothelial NOS knockout mice. Am J Physiol 1998;274:H411-5.
26. Miyagoe-Suzuki Y, Takeda S. Association of neuronal nitric oxide synthase (nNOS) with α1-syntrophin at the sarcolemma. Microsc Res Tech 2001;55:164-70.
27. Boegehold MA. Flow-dependent arteriolar dilation in normotensive rats fed low- or high-salt diets. Am J Physiol 1995;269:H1407-14.
28. Sun D, Huang A, Smith CJ, et al. Enhancing release of prostaglandins contributes to flow-induced arteriolar dilation in eNOS knockout mice. Circ Res 1999;85:288-93.
29. Koller A, Sun D, Kaley G. Role of shear stress and endothelial prostaglandins in flow- and viscosity-induced dilation of arterioles in vitro. Circ Res 1993;72:1276-84.
30. Wehling M, Spencer MJ, Tidball JG. A nitric oxide synthase transgene ameliorates muscular dystrophy in *mdx* mice. J Cell Biol 2001;155:123-31.
31. Lau KS, Grange RW, Chang WJ, et al. Skeletal muscle contractions stimulate cGMP formation and attenuate vascular smooth muscle myosin phosphorylation via nitric oxide. FEBS Lett 1998;431:71-4.
32. Leinonen H, Juntunen J, Somer H, et al. Capillary circulation and morphology in Duchenne muscular dystrophy. Eur Neurol 1979;18:H714-21.
33. Asai A, Sahani N, Kaneki M, et al. Primary role of functional ischemia, quantitative evidence for the two-hit mechanism, and phosphodiesterase-5 inhibitor therapy in mouse muscular dystrophy. PLoS ONE 2007;29:e806.

CELL STRUCTURE AND FUNCTION 33: 163–169 (2008)

MicroRNA-206 Is Highly Expressed in Newly Formed Muscle Fibers: Implications Regarding Potential for Muscle Regeneration and Maturation in Muscular Dystrophy

Katsutoshi Yuasa[1], Yasuko Hagiwara[1], Masanori Ando[2], Akinori Nakamura[3], Shin'ichi Takeda[3], and Takao Hijikata[1]*

[1]Department of Anatomy and Cell Biology, and [2]Department of Environmental Science, Research Institute of Pharmaceutical Science, Faculty of Pharmacy, Musashino University, Nishitokyo, Tokyo 202-8585, Japan and [3]Department of Molecular Therapy, National Institute of Neuroscience, NCNP, Tokyo 187-8502, Japan

ABSTRACT. **miR-1, miR-133a, and miR-206 are muscle-specific microRNAs expressed in skeletal muscles and have been shown to contribute to muscle development. To gain insight into the pathophysiological roles of these three microRNAs in dystrophin-deficient muscular dystrophy, their expression in the tibialis anterior (TA) muscles of *mdx* mice and CXMD$_J$ dogs were evaluated by semiquantitative RT-PCR and *in situ* hybridization. Their temporal and spatial expression patterns were also analyzed in C2C12 cells during muscle differentiation and in cardiotoxin (CTX)-injured TA muscles to examine how muscle degeneration and regeneration affect their expression. In dystrophic TA muscles of *mdx* mice, miR-206 expression was significantly elevated as compared to that in control TA muscles of age-matched B10 mice, whereas there were no differences in miR-1 or miR-133a expression between B10 and *mdx* TA muscles. On *in situ* hybridization analysis, intense signals for miR-206 probes were localized in newly formed myotubes with centralized nuclei, or regenerating muscle fibers, but not in intact pre-degenerated fibers or numerous small mononucleated cells, possibly proliferating myoblasts and inflammatory infiltrates. Similar increased expression of miR-206 was also found in C2C12 differentiation and CTX-induced regeneration, in which differentiated myotubes or regenerating fibers showed abundant expression of miR-206. However, CXMD$_J$ TA muscles contained smaller amounts of miR-206, miR-1, and miR-133a than controls. They exhibited more severe and more progressive degenerative alterations than *mdx* TA muscles. Taken together, these observations indicated that newly formed myotubes showed markedly increased expression of miR-206, which might reflect active regeneration and efficient maturation of skeletal muscle fibers.**

Key words: microRNA/miR-206/muscular dystrophy/muscle regeneration

Introduction

MicroRNAs (miRNAs) are small, ~22-nucleotide, non-coding RNA molecules that post-translationally regulate gene expression. Many miRNAs are expressed in a tissue-specific manner, and seem to contribute to tissue specification during differentiation (Mansfield *et al.*, 2004; Hornstein *et al.*, 2005; Lagos-Quintana *et al.*, 2002; Chang *et al.*, 2004; Fazi *et al.*, 2005). In addition, they have been implicated in the pathogenesis of cancers and infectious diseases (for review, see Boyd, 2008; Iorio *et al.*, 2005; Jopling *et al.*, 2005).

The three muscle-specific miRNAs, miR-1, miR-133, and miR-206 have been shown to play important roles in the regulation of muscle development. miR-1 and miR-133 are expressed in cardiac and skeletal muscle and are transcriptionally regulated by the myogenic differentiation factors, such as MyoD, myogenin, Mef2, and serum response factor (SRF) (Rao *et al.*, 2006; Chen *et al.*, 2006; Kwon *et al.*, 2005; Sokol and Ambros, 2005; Zhao *et al.*, 2005). miR-1 promotes differentiation of cardiac and skeletal progenitors and their exit from the cell cycle in mammals (Zhao *et al.*, 2005, 2007; Kwon *et al.*, 2005), while miR-133 inhibits

*To whom correspondence should be addressed: Takao Hijikata, Department of Anatomy and Cell Biology, Faculty of Pharmacy, Research Institute of Pharmaceutical Sciences, Musashino University, 1-1-20 Shinmachi Nishitokyo-shi, Tokyo 202-8585, Japan.
Tel & Fax: +81-42-468-9290
E-mail: hijikata@musashino-u.ac.jp

Abbreviations: CTX, cardiotoxin; CXMD$_J$, canine X-linked muscular dystrophy in Japan; DMD, Duchenne muscular dystrophy; *mdx*, X chromosome-linked muscular dystrophy; RT-PCR, reverse transcription polymerase chain reaction; TA, tibialis anterior.

their differentiation and maintains them in a proliferative state (Chen *et al.*, 2006). miR-206 is expressed only in skeletal muscles, and its expression appears to be induced by MyoD and myogenin during myogenesis and promotes muscle differentiation (Kim *et al.*, 2006; Rosenberg *et al.*, 2006). These muscle-specific miRNAs also seem to participate in muscle diseases, including cardiac hypertrophy, heart failure, cardiac arrhythmias, congenital heart disease, and muscular dystrophy (Carè *et al.*, 2007; van Rooij *et al.*, 2006, 2007; Yang *et al.*, 2007; McCarthy *et al.*, 2007; Eisenberg *et al.*, 2007).

To gain insight into the pathophysiological roles of muscle-specific miRNAs in dystrophin-deficient muscular dystrophy, we analyzed the profiles of miR-1, miR-133a, and miR-206 expression in TA muscles of *mdx* mice and CXMD$_J$ dogs by semiquantitaive RT-PCR and *in situ* hybridization. In addition, their temporal and spatial expression patterns were examined in C2C12 cells during myogenesis and in tibialis anterior (TA) muscles during a degeneration-regeneration process induced by cardiotoxin (CTX)-injury. Here, we demonstrated that miR-206 was highly expressed within muscle fibers newly formed from satellite cells during regeneration in CTX-injured and dystrophic *mdx* muscles. However, miR-206 was not abundantly expressed in CXMD$_J$ TA muscles, which exhibited much more severe and progressive degeneration than those of *mdx* mice. The degree of miR-206 expression might depict the potential of muscle regeneration and maturation.

Material and Methods

Animals and tissue preparation

The use of animals was approved by the Animal Ethics Committee of Musashino University or the Ethics Committee for Treatment of Laboratory Animals at NCNP. Three-week-old to one-year-old male control (strain C57BL/10; B10) and *mdx* mice were anesthetized with diethyl ether and sacrificed by cervical dislocation to dissect out the TA muscles. For regeneration assay, injury was performed on TA muscles of 12-week-old C57BL/6 (B6) mice by injecting 100 μl of 10 μM cardiotoxin (CTX). Mice were sacrificed at 1, 2, 3, 4, 5, and 7 days, 2, 4, and 8 weeks post-injection to collect the TA muscles. Wild-type and dystrophic CXMD$_J$ dogs were sacrificed by exsanguination under anesthesia with isoflurane to dissect out the TA muscles.

Cell culture

C2C12 myoblasts were cultured on the collagen-coated dishes in growth medium consisting of DMEM and 20% fetal calf serum. Differentiation into myotubes was induced by switching the culture medium to differentiation medium consisting of 5% horse serum and 10 μg/ml insulin in DMEM, followed by culture for 1, 3, or 6 days.

Quantification of miRNA expression and statistical analyses

Muscle-specific miR-1, miR-133a, and miR-206 were quantified by real-time reverse transcription polymerase chain reaction (RT-PCR) using total RNA obtained from C2C12 cells and TA muscles as well as a TaqMan MicroRNA Assay kit (Applied Biosystems). Each miRNA expression was represented relative to the expression of small RNA U6 used as an internal control in RT-PCR. Expression data were given as means of relative expression values obtained from three samples in conjunction with standard deviation. Statistical comparisons were performed by t-test or Aspin-Welch-test.

In situ hybridization

In situ hybridization was performed using a locked nucleic acid (LNA) detection probe for mmu-mir-206 (Exiqon), which was labeled with digoxigenin (DIG) using a DIG oligonucleotide tailing kit (Roche). C2C12 cells fixed with 4% paraformaldehyde (PFA) in PBS were immersed in 100% methanol, rehydrated, treated with proteinase K, and then re-fixed with PFA, whereas cryosections prepared from TA muscles fixed with 4% PFA were treated with proteinase K, re-fixed with PFA, and then acetylated with acetylation buffer (0.1 M triethanolamine pH 8.0). After washing with PBS, both types of specimen were incubated with DIG-labeled miR-206 probes at 55°C overnight. After stringent wash at 55°C in 50% formamide, 2×SSC, 0.1% Tween-20, and at room temperature in 0.2×SSC and then PBS, they were incubated with blocking solution, followed by alkaline phosphatase-conjugated anti-DIG antibody (Roche). Hybridized probes were detected and visualized by color reaction with nitroblue tetrazolium (NBT) and 5-bromo 4-chloro-3-indolyl phosphate (BCIP).

Results

Using RT-PCR Taqman assay, we analyzed the expression profiles of miR-1, miR-133a, and miR-206 in TA muscles from control B10 and dystrophic *mdx* mice at different ages. As shown in Fig. 1A, miR-206 was constantly expressed in *mdx* TA muscles throughout the ages examined from 3 weeks to 1 year, whereas its expression was reduced with age in control B10 muscles. Thus, a comparison between age-matched B10 and *mdx* mice indicated significantly increased expression of miR-206 in *mdx* TA muscles. On the other hand, there were no differences in the expression of miR-1 or miR-133a between B10 and *mdx* mice at any age examined except at 5 and 8 weeks old, when *mdx* TA muscles showed slightly reduced expression of miR-133a as compared to B10 TA muscles.

Next, to identify which types of cells abundantly express miR-206 within *mdx* TA muscle, *in situ* hybridization analysis was performed by using DIG-labeled miR-206 probes. Intense signals for miR-206 probes were observed in newly

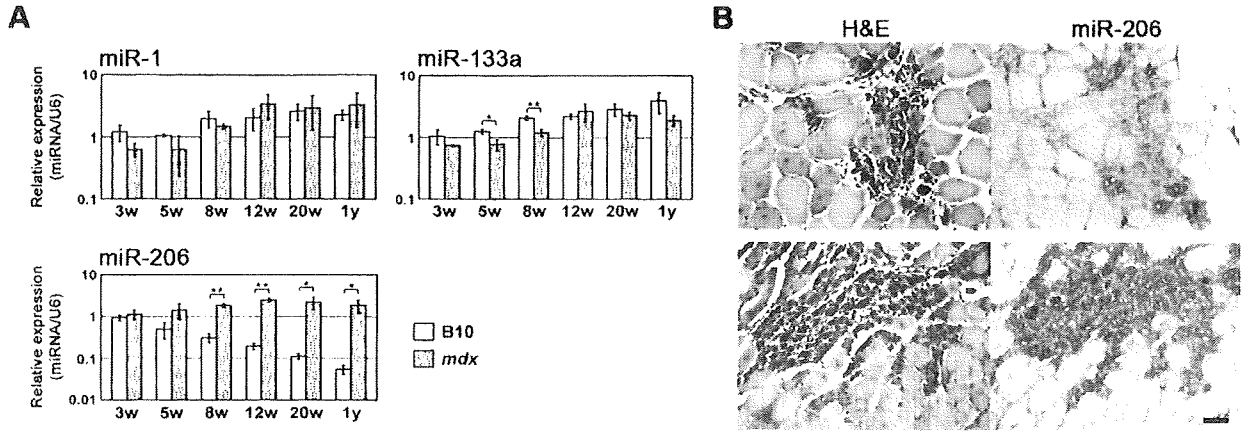

Fig. 1. **A**, Expression levels of miR-1, miR-133a, and miR-206 in TA muscles of *mdx* and B10 mice at different ages. All expression levels were determined by real-time RT-PCR. Results are presented as mean relative expression±SD; n=3. *, P<0.05; **, P<0.01. **B**, Serial cross-sections from TA muscles of 8-week-old *mdx* mice. *In situ* hybridization using miR-206 probes on one section (right) and hematoxylin and eosin (H&E) staining on an adjacent section (left). *In situ* hybridization analyses showed intense signals for miR-206 probes in newly formed muscle fibers with centralized nuclei, or regenerating fibers. Bar, 50 μm.

formed myotubes and immature muscle fibers with centralized nuclei, or regenerating muscle fibers (Fig. 1B). However, intact (pre-degenerated) muscle fibers and many small mononucleated cells, such as inflammatory infiltrates, fibroblasts, and proliferating satellite cells, appeared to lack miR-206 signals. These results clearly indicated that increased expression of miR-206 in *mdx* TA muscles was due to newly formed muscle fibers. For control experiments, the tissue sections were hybridized with LacZ probes or treated without miR-206 probes, thereby presenting no specific and positive signals.

To compare to the results obtained in *mdx* TA muscles, the expression levels of the three miRNAs were analyzed in TA muscles from wild-type or CXMD$_J$ dogs. CXMD$_J$ dogs exhibit a much more severe and more progressive dystrophic form than *mdx* mice and almost recapitulate dystrophinopathy phenotype DMD in human (Shimatsu *et al.*, 2005). As shown in Fig. 2, CXMD$_J$ TA muscles expressed smaller amounts of miR-1, miR-133a, and miR-206 than wild-type controls. These reduced levels of expression in CXMD$_J$ TA muscles, as assessed by semiquantitaive RT-PCR from total RNA, may represent either a decrease in the number of cells expressing the three muscle-specific miRNAs or in the amount of miRNA per cell. The former is likely, since CXMD$_J$ TA muscles contain many degenerated muscle fibers, inflammatory infiltrates, and fibroblasts (Fig. 3A), none of which express muscle-specific miRNAs. To assess the latter, i.e., whether CXMD$_J$ muscle fibers, including those in the process of regenerating, express smaller amounts of miR-206 than muscle fibers of wild-type dogs or *mdx* mice, we calculated the relative levels of expression of miR-206 and miR-133 to miR-1, which was induced only in differentiated myotubes (Rao *et al.*, 2006). As shown in

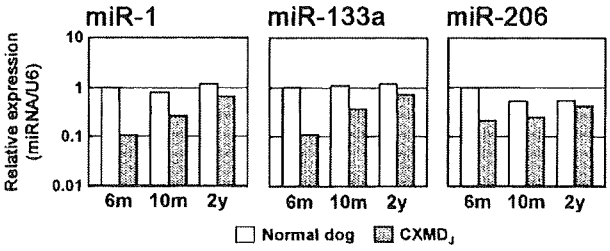

Fig. 2. Expression levels of miR-1, miR-133a, and miR-206 in TA muscles of CXMD$_J$ and wild-type dogs at different ages (n=1 at each age).

Fig. 3B, the relative expression of miR-206 to miR-1 was elevated in CXMD$_J$ TA muscles as compared to controls. However, CXMD$_J$ muscles did not exhibit such a marked increase in relative expression of miR-206 as observed in *mdx* muscles (Fig. 3C). On the other hand, the expression of miR-133a relative to that of miR-1 showed a similar ratio of around 1 as compared between mice and dogs.

As shown above, dystrophic TA muscles contain many degenerating and regenerating muscle fibers as well as inflammatory infiltrates. These observations prompted us to assess how muscle degeneration and regeneration affect the expression of miR-1, miR-133a, and miR-206. The temporal and spatial expression patterns of these miRNAs were analyzed in C2C12 cells during muscle differentiation as an *in vitro* model of muscle regeneration, and in cardiotoxin (CTX)-injured TA muscles as an *in vivo* model of the degeneration-regeneration process. The degeneration-regeneration process induced by CTX-injury was well documented as follows: After CTX injection, satellite cell proliferation occurs within 2 days, myogenic differentiation